Journal of Asian Earth Sciences 49 (2012) 376–395

Contents lists available at SciVerse ScienceDirect

Journal of Asian Earth Sciences

journal homepage: www.elsevier.com/locate/jseaes

Intracontinental orogenesis in an ancient continent–continent collision zone: Evidence from structure, metamorphism and P-T paths across a suspected suture zone within the Eastern Ghats Belt, India

Jagatbikas Nanda, Saibal Gupta *

Dept. of Geology and Geophysics, Indian Institute of Technology, Kharagpur 721 302, India

ARTICLE INFO

Article history:
Available online 25 November 2011

Keywords:
Jeypore Province
Eastern Ghats
Intracontinental orogenesis
Reworking
Granulites

ABSTRACT

In the Eastern Ghats Belt of India, deformation and granulite facies metamorphism are generally correlated with India–Antarctica collision during the assembly of Rodinia. Within the belt, Archean granulites in the west are separated from Proterozoic granulites to the east by a prominent lithotectonic contact. Recent studies assume this contact to be the suture zone related to collision, although the structural and metamorphic evolution of the Archean granulites are so far undescribed. In this study, an integrated structural and metamorphic study conducted across the contact reveals that each unit preserves unrelated early granulite facies fabrics, but subsequently shared a top-to-the-west thrusting event that imprinted a penetrative NE–SW trending, southeasterly dipping shear foliation along the boundary zone. Syn-thrusting fluid infiltration initially stabilized hydrous minerals at the cost of earlier granulite facies assemblages in both units. Renewed heating and loading then re-established granulite facies conditions in both units, with peak conditions around 8 kb, 750–800 °C, possibly in the mid-Neoproterozoic time. Since metamorphic conditions and P-T trajectories are similar across the contact, the pre-thrusting thermal structure in both units is inferred to be similar. This implies that both units were already amalgamated into a common footwall block prior to this shared tectonothermal event. No ophiolites, arc magmas or post-collisional granitic activity of Neoproterozoic age are associated with this contact. It is concluded that the contact between Archean and Proterozoic granulites in the Eastern Ghats Belt is not a suture but records intracontinental orogenesis within the collision belt that either predates or post-dates the Proterozoic India–Antarctica amalgamation.

1. Introduction

Paleomagnetic, geochronologic, and petrologic evidence (e.g. Hoffman, 1989; Unrug, 1996; Meert, 2002; Meert et al., 2011; Rogers and Santosh, 2002, 2009; Boger, 2011) supports the idea that supercontinents grew by amalgamating disparate cratonic blocks or terranes along intensely deformed and metamorphosed mobile belts (e.g. Zhao et al., 2002; Collins and Pisarevsky, 2005; Santosh et al., 2009; Santosh, 2010). The Indian shield became a part of the Neoproterozoic (~1300–900 Ma) supercontinent Rodinia (Dalziel, 1991; Hoffman, 1991; Moores, 1991; Li et al., 2008) following continental collision with a fragment of East Antarctica, around 900 Ma (Li et al., 2008). This collision is believed to have occurred along the eastern fringe of the Archean cratonic nucleus of Peninsular India that is now represented by the Eastern Ghats Belt (EGB, Fig. 1a). At present, the EGB is preserved as a granulite facies mobile belt that has geological affinity with, and is therefore assumed to have been contiguous with the Rayner Province in East Antarctica from 1000 to 900 Ma (Mezger and Cosca, 1999; Boger et al., 2000, 2001; Fitzsimons, 2000; Kelly et al., 2002). From this perspective, the Indian craton–EGB contact must represent a Proterozoic suture zone, and is therefore of great significance to the assembly of the Rodinia supercontinent.

The structural and metamorphic evolution of the EGB assumes great importance in the context of this collision event. Earlier geological studies have already established that the EGB is multiply deformed and poly-metamorphic (Gupta, 2004; Chetty, 2010). Subsequent geochronological studies have however demonstrated that major thermal events within the belt occurred at different times (see Mukhopadhyay and Basak, 2009; Gupta, in press), implying that all deformational and metamorphic events within the belt cannot be attributed to the India–Antarctica collision. Thus, in order to isolate components of the P-T evolution that are an outcome of the collisional event, it is also necessary to identify the events that are not related to the collision. In this study, we identify one such area within the EGB where Archean and Proterozoic granulites

* Corresponding author. Tel.: +91 03222 283370; fax: +91 03222 255303.
E-mail addresses: jagatbikas@gmail.com (J. Nanda), saibl2008@gmail.com (S. Gupta).

1367-9120/$ - see front matter © 2011 Elsevier Ltd. All rights reserved.
doi:10.1016/j.jseaes.2011.10.001

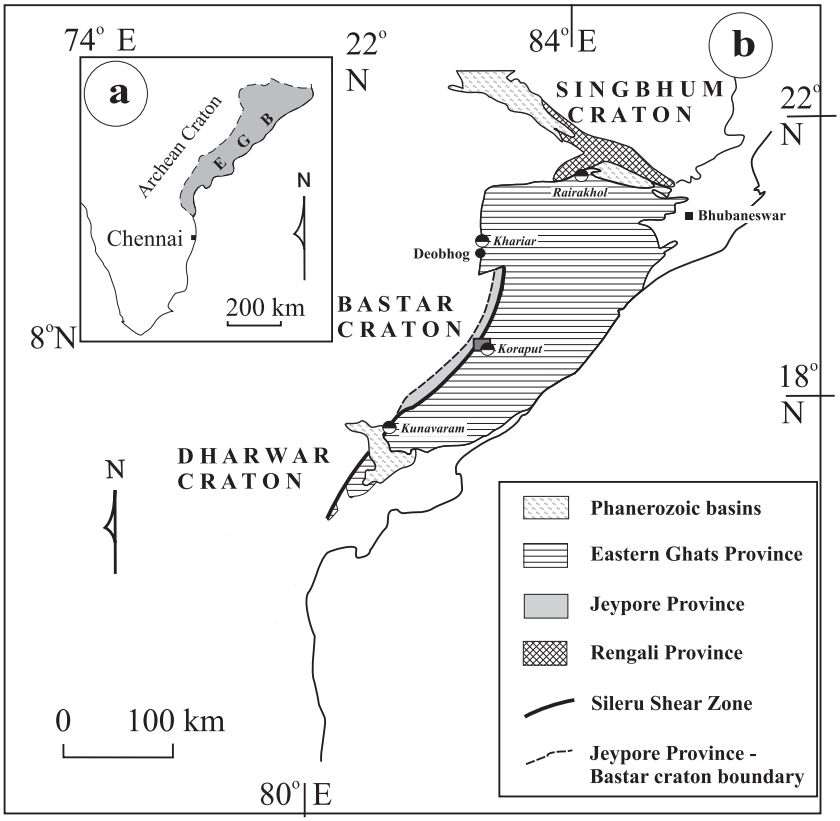

Fig. 1. (a) Location of the Eastern Ghats Belt (shaded) in peninsular India; (b) Geological sub-division of the EGB (after Dobmeier and Raith, 2003) showing the respective locations of the EGP and Jeypore Province within the EGB. Note that the Archean craton (Bastar) *sensu stricto* lies geographically west of the Jeypore Province. The study area (see box around Koraput) straddles the boundary between Jeypore Province and EGP. Note that the alkaline complexes at Rairakhol, Khariar and Kunavaram are aligned precisely along the contact between granulitic and non-granulitic (i.e. craton *sensu stricto*) terraines. Only the alkaline complex at Koraput lies entirely within granulites of the EGP. Also note that west of Koraput, the Sileru Shear Zone separates two granulitic suite of rocks (i.e. the Jeypore Province and the EGP). In this sector, the western boundary of the Jeypore Province (dashed line) represents the contact between the granulitic and non-granulitic components.

are separated by a major lithotectonic contact, that has been considered by some workers to be a collisional suture. In this study, we present the first document of a metamorphic P-T path from the Archean unit, and demonstrate its similarity with that in the Proterozoic granulites across the contact. We identify a set of criteria based on which the collisional signature has been recognized in various parts of the EGB-craton contact, and argue that the structure and metamorphism documented in this study are not related to a collisional event, and must therefore be a product of intracontinental orogenesis.

2. Geological background

The EGB is recognized as a mobile belt within which lithologic domains are oriented parallel to the trend of the belt (Narayanaswami, 1975; Nanda and Pati, 1989; Ramakrishnan et al., 1998). Recent geological and geochronological data (Rickers et al., 2001; Kovach et al., 2001; Dobmeier and Raith, 2003) demonstrate that the EGB is not a homogeneous unit, but comprises discrete provinces with distinct geological histories (see Dobmeier and Raith, 2003; Gupta, 2004; Vijaya Kumar and Leelanandam, 2008; Mukhopadhyay and Basak, 2009 for reviews). Of particular importance in the context of this study is the contact between the charnockitic suite that occupies the western fringe of the EGB, and the dominantly metasedimentary unit comprising quartzofeldspathic gneisses, garnet–sillimanite (metapelitic) gneisses, calc-gneisses and high Mg–Al granulites that are intruded by megacrystic granitoids. Available age data suggest that the last significant thermal impression on the charnockites/charno-enderbites/enderbites occurred in the Archean time (Kovach et al., 2001; Simmat and Raith, 2008); this fringe zone was designated as the 'Jeypore Province' (Figs. 1b and 2) by Dobmeier and Raith (2003). In contrast, the meta-sediments and plutonic intrusives to the east of the Jeypore Province underwent high grade metamorphism in the Grenvillian time, with a strong Pan-African thermal overprint (Mezger and Cosca, 1999; Dobmeier and Raith, 2003; Simmat and Raith, 2008). This zone occupies the major part of the EGB (Figs. 1b and 2), and was referred to as the 'Eastern Ghats Province' (EGP, Fig. 2) by Dobmeier and Raith (2003). The metamorphic evolution of this province is documented (see Dasgupta and Sengupta, 2003, for summary), and is broadly believed to have been subjected to an early M1 phase (1.2–1.1 Ga; Simmat and Raith, 2008) of UHT metamorphism (~8–10 kb, 1000 °C) that was characterized by an isobaric heating–cooling trajectory (Sengupta et al., 1990; Dasgupta et al., 1995). This was followed by a second granulite facies imprint (M2, ~8–8.5 kb, 850 °C; Dasgupta et al., 1992, 1995) that was accompanied by pervasive regional deformation (Dobmeier and Raith, 2003), penetrative fabric formation and intrusion of megacrystic granitoids in the period 980–930 Ma (Grew and Manton, 1986; Aftalion et al., 1988; Paul et al., 1990; Shaw et al., 1997; Mezger and Cosca, 1999). The M2 peak was supposedly followed by near-isothermal decompression (Dasgupta and Sengupta, 2003). Recent studies (e.g. Korhonen et al., 2011) suggest that the post-peak temperature path following UHT also involved decompression, and that the two granulite events may be temporally indistinguishable. A final thermal overprint (M3) in the amphibolite facies is recorded at ~550 Ma (Mezger and Cosca, 1999). The metamor-

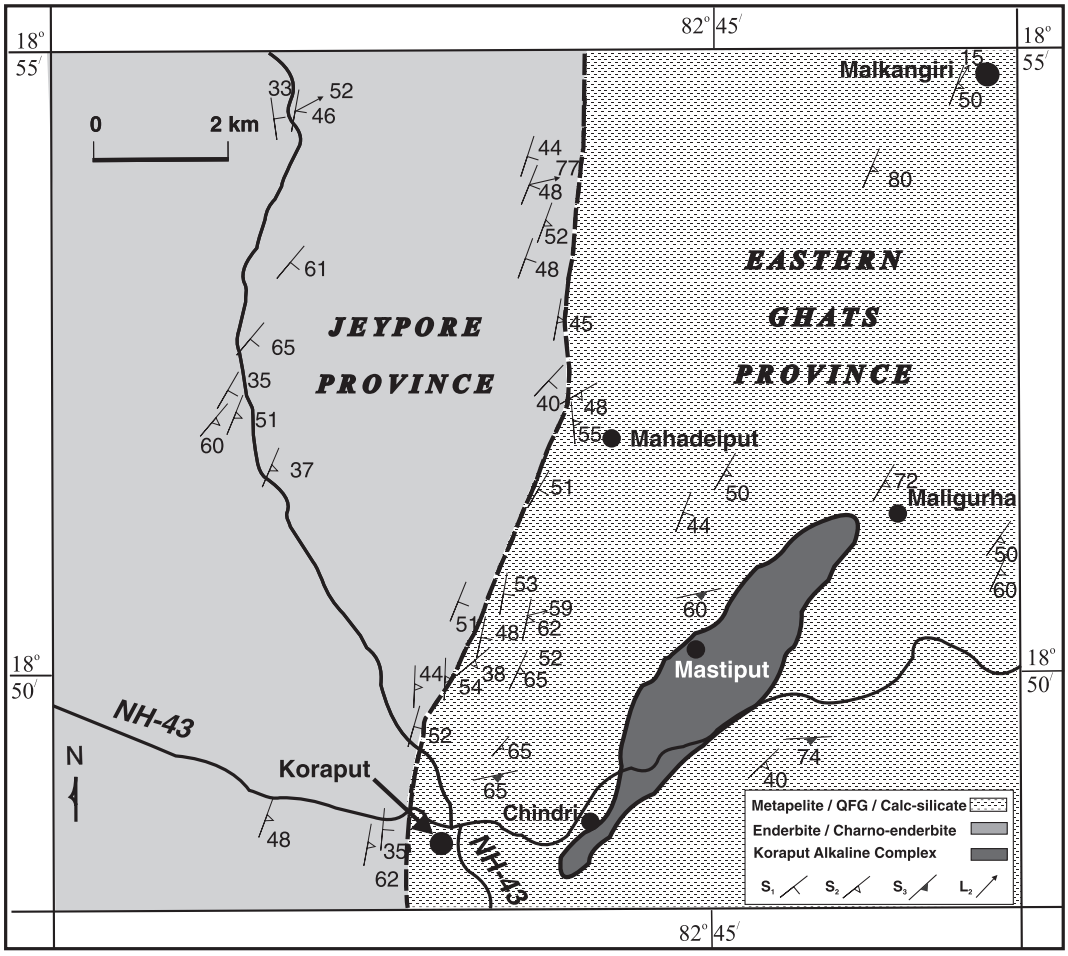

Fig. 2. Disposition of the major lithological units in the study area. The Jeypore Province unit is composed of charnockites, charno-enderbites and enderbites, while the EGP unit includes quarzofeldspathic, metapelitic and calc-silicate gneisses. The alkaline pluton at Koraput is intrusive into the EGP rocks.

phic ensemble, P-T evolution and ages of metamorphism in the EGP are remarkably similar to the Rayner Province of East Antarctica (Mezger and Cosca, 1999; Harley, 2003), and the two spatially disparate terranes are, therefore, widely considered to have been contiguous in the supercontinent Rodinia.

In contrast to the EGP, much less information is available about the metamorphic history of the Jeypore Province. The charnockitic suite of this province includes charnockites, charno-enderbites and enderbites with rocks of intermediate composition dominating (Dobmeier and Raith, 2003). Mafic granulites generally occur as disrupted bands, lenses or xenoliths, although regionally extensive bands are also occasionally present (Nanda and Pati, 1989). Subbarao et al. (1998) concluded from geochemical studies that these mafic granulites hosted within the charnockite suite of rocks originated through limited fractionation of rift related tholeiitic–intermediate magmas, although Dobmeier and Raith (2003) interpreted the enderbite magmatism to be arc-related, based on the preponderance of intermediate rocks with calc-alkaline affinity. The enderbites/charnoenderbites were characterized by Archean Nd model ages (Kovach et al., 2001; Rickers et al., 2001). Pressure–temperature conditions during subsequent metamorphism were constrained within the range 630–780 °C at pressures of 5.5–5.6 kb from a limited number of garnetiferous mafic granulite samples (Subbarao et al., 1998), but there were no constraints on the associated P-T path. U–Pb data from complexly zoned zircon grains suggest a last thermal imprint at ~2.8 Ga (Kovach et al., 2001). Thus, although information on the Jeypore Province is limited, the P-T conditions of metamorphism and the Archean ages point to a clear distinction from the granulites of the EGP.

South of the Godavari, the contact between the Dharwar craton and the EGB granulites appears as a prominent lineament on Landsat images (the 'Sileru Shear Zone' of Chetty and Murthy, 1993, 1994; Fig. 1) and preserves characteristics of a suture zone (see Section 9.4). North of the Godavari, the contact between the Archean age (Sarkar et al., 1993) amphibolite facies lithologies of the Bastar craton and the EGB granulites coincides with the western boundary of the 'Western Charnockite Zone' of the EGB (WCZ; Walker, 1902; Fermor, 1936; Crookshank, 1938; Narayanaswami, 1975; Ramakrishnan et al., 1998). However, based on the apparent distinction in metamorphic conditions and ages, Dobmeier and Raith (2003) redesignated the WCZ as the 'Jeypore Province', and considered it to be part of the Bastar cratonic foreland that collided with the rest of the Eastern Ghats Belt (i.e. the EGP) in the Pan-African time (Simmat and Raith, 2008). This implies that north of the Godavari, the Bastar craton-EGB contact or suture zone should coincide with the Jeypore Province–Eastern Ghats *Province* boundary (i.e. between two granulite provinces), rather than the Bastar craton (*sensu stricto*)-Jeypore Province (or WCZ) contact. This study has been conducted along a transect across the EGP–Jeypore Province contact (Fig. 1b, shown by gray colored box), and is ideally located for evaluating the evidence for a suture.

3. Geology of the study area

The Jeypore Province unit in the transect is dominated by a suite of charnockitic rocks that comprise greasy green, coarse to medium grained, equigranular charnockites, charno-enderbites and enderbites (Subbarao et al., 1998; Kovach et al., 2001). These lithologies occur in close spatial association and cannot be separately mapped (Fig. 2). All these rocks are characterized by well developed gneissic layering (Fig. 3a). Mafic granulites are present as lenticular enclaves (Fig. 3a) or disrupted bands within the charnockitic suite host rock. East of the Jeypore Province, rocks of the Eastern Ghats Province are dominated by characteristically weathered garnet–sillimanite, quartzofeldspathic and calc-silicate gneisses that are intruded by orthopyroxene-bearing megacrystic granitoids. Along the studied transect, structural and metamorphic evolution of the rocks of the EGP unit, including the Koraput Alkaline Complex (KAC), have been described in detail by Gupta et al. (2005), Nanda et al. (2008) and Nanda et al. (2009), and is summarized below. These studies have established that an early event of granulite facies metamorphism with associated fabric formation in EGP was followed by intrusion of the alkaline pluton at Koraput (~3 km east of the contact between EGP and Jeypore Province; Fig. 2). Thereafter, the high grade assemblages retrogressed into the amphibolite facies concomitantly with hydrous fluid infiltration. This metamorphism was also accompanied by penetrative shearing on a regional scale along a north-easterly trending, south-easterly dipping foliation. Subsequently, the entire area underwent renewed heating followed by loading, culminating in a second granulite facies metamorphic event that peaked at ~8.0 kb, 700 °C (Nanda et al., 2008).

4. Structural evolution across the Jeypore Province–EGP contact

The charnockite suite of rocks occurring along the eastern margin of the Jeypore Province experienced three phases of deformation (designated as D_{1JP}, D_{2JP}, and D_{3JP}). The earliest D_{1JP} deformation caused the development of the gneissic foliation (S_{1JP}) defined by alternating leucocratic layers composed of flattened/ribbon quartz + deformed plagioclase grains that show a preferred dimensional orientation, and meso- to melanocratic layers composed of lenticular aggregates of orthopyroxene ± amphibole ± biotite ± clinopyroxene. In places, the compositional layers (S_{1JP}) curve into a NNE-trending, easterly dipping later shear foliation S_{2JP} that is interpreted to be related to a second deformation event, D_{2JP}. S_{2JP} (Fig. 3a) is defined by the same mineral assemblages as S_{1JP}, but with a relative increase in the modal proportion of hydrous phases, i.e. biotite and hornblende. Along the contact zone between the Jeypore Province and the EGP S_{2JP} is more penetrative, with S_{1JP} being tightly folded and rotated parallel to the S_{2JP} shear foliation. Foliation development (S_{3JP}) during the D_{3JP} shearing event is restricted to some narrow, almost E–W trending shears that dip steeply towards south. Within these narrow shear bands, the modal proportion of biotite and hornblende is even higher.

Metapelitic gneisses, quartzofeldspathic gneisses and megacrystic granitoids of the EGP to the east of the contact with the Jeypore Province also experienced three deformation events. In this study, the subscript 'EG' has been used for the EGP rocks; these correspond to the 'CR' fabrics defined in Nanda et al. (2008, 2009). The earliest deformation event in these rocks, D_{1EG}, resulted in the S_{1EG} segregation layering, defined by orthopyroxene + biotite – bearing layers in quartzofeldspathic gneisses (Fig. 3b) and biotite + sillimanite – bearing layers in metapelitic gneisses (Fig. 3c). S_{1EG} is completely transposed parallel to a NE–SW trending, east dipping S_{2EG} fabric during the regional scale D_{2EG} shearing event (Gupta et al., 2005). S_{1EG} and S_{2EG} are essentially defined by the same minerals, and can only be distinguished in places where S_{1EG} is observed curving into S_{2EG}. A final phase of shearing resulted in the formation of an E–W trending, steeply south dipping S_{3EG} foliation within narrow shear bands.

The S_{2JP} foliation in the Jeypore Province is concordant with the second generation S_{2EG} shear foliation in the adjacent

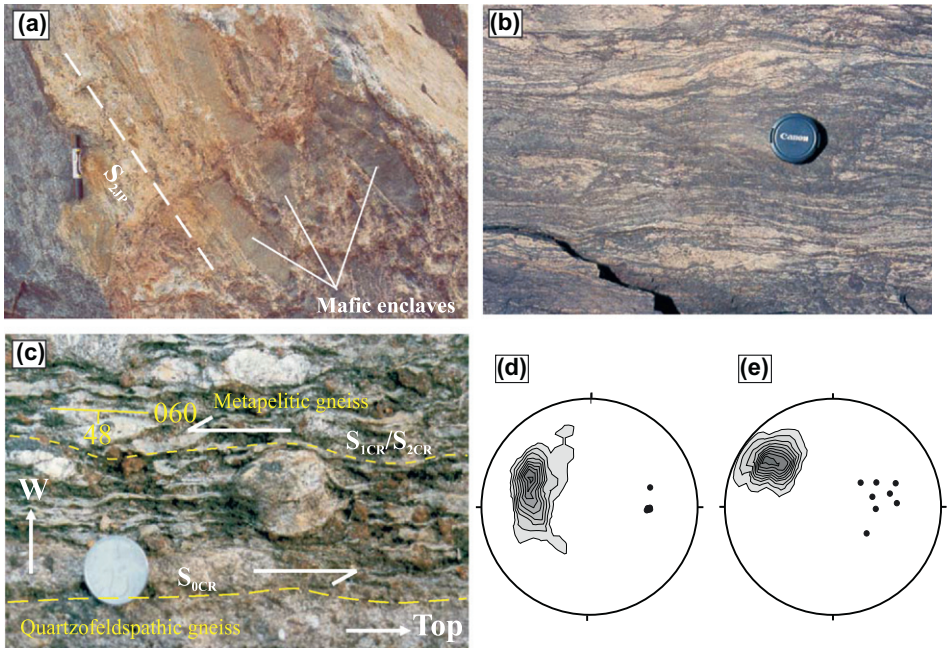

Fig. 3. (a) Field photograph of the S_{2JP} foliation in a charno-enderbite of the Jeypore Province along with lenticular, mafic-rich enclaves (marker pen length = 6 in. (b) S_{1EG} gneissic foliation in metapelitic gneiss of the EGP unit, adjacent to the contact between the EGP and the Jeypore Province (lens cap diameter = 6 cm). (c) S_{1EG} gneissic foliation wrapping around Grt porphyroblasts in metapelitic gneiss of the EGP unit. (d) Contoured equal area plots of the poles to the S_{1JP} and S_{2JP} foliations (n = 27) in the Jeypore Province unit showing concentration around a pole corresponding to a plane oriented at 023° /54°E. The solid dots represent lineation data (n = 6). (e) Contoured qual area plots of the poles to the S_{1EG} and S_{2EG} foliations (n = 106) in the EGP unit. Note that the foliation maximum (033°/60°E) and the distribution of the lineation data (solid dots, n = 8) are similar to that in the Jeypore Province.

garnet–sillimanite gneisses and quartzofeldspathic gneisses of the EGP. Equal area plots of the poles to the S_{1JP} and S_{2JP} foliations (Fig. 3d) show a small scatter, but with a maximum around a mean orientation of 023°/54°E, consistent with the mean orientation (033°/60°E) of S_{2EG} (Fig. 3e). The scatter in Fig. 3d reflects the incomplete transposition of S_{1JP} in the Jeypore Province towards the S_{2JP} maximum further west of the contact; in the EGP unit, the transposition is more complete. In most cases, a down-dip quartz mineral lineation is associated with S-C fabrics; asymmetric clasts in vertical sections perpendicular to the shear foliation invariably indicate a top-to-the-west movement sense (Fig. 3c).

5. Petrography, microstructure and mineral chemistry of rocks in the contact zone

The mineral chemical data presented in this section were acquired on a CAMECA SX-100 machine at the EPMA Laboratory in the Central Petrological Laboratories, of the Geological Survey of India, Kolkata and in the laboratory of Indian Bureau of Mines, Ore Dressing Division, Nagpur. An accelerating voltage of 15 kV, and a beam current of 15 nA were used in the former case, while a beam current of 15 kV and sample beam current of 12nA were used in later. In all cases, the beam size was 1 μm. The abbreviations used in the text for describing the petrography and mineral chemistry are according to the Kretz (1983) except in Figs. 6 and 7, where abbreviations for end members are according to the THERMOCALC (v. 3.26) program.

5.1. Jeypore Province

The charnockitic suite of rocks (charnockites, enderbites and charnoenderbites) of this province comprises plagioclase, quartz, orthopyroxene, clinopyroxene, garnet, hornblende, ilmenite, K-feldspar, and biotite. Among these minerals hornblende, clinopyroxene, biotite, K-feldspar and garnet proportions show wide spatial variation. Rutile, zircon and apatite are accessories. Along the contact with EGP, the enderbite/charno-enderbite is well foliated and mylonitised, characterized by ribbon/flattened quartz with chessboard (Fig. 4a) structures that suggest high temperature deformation (Kruhl, 1996). In places, deformed plagioclase and orthopyroxene show preferred alignment along the S_{1JP} and S_{2JP} (Fig. 4b) foliation. This foliation anastomoses around porphyroclasts of plagioclase, K-feldspar and antiperthite. In recrystallised domains, quartz–quartz and plagioclase–plagioclase contacts are wavy indicating grain boundary migration. In the melanocratic layers, garnet porphyroblasts are annealed (Fig. 4c) into the S_{2JP} foliation along with orthopyroxene, ilmenite, plagioclase, and quartz or over grow the S_{3JP} foliation (Fig. 4d). **Plagioclase** mainly constitutes the matrix. Sub-rounded to rounded inclusions also occur within garnet in association with clinopyroxene and quartz. There is no grain-scale compositional variation within the plagioclase, though a wide variation in anorthite content (X_{Ca} 0.53–0.56, X_{Na} 0.43–0.46; to X_{Ca} 0.36–0.39, X_{Na} 0.59–0.62; see Table 1, samples K279 and K280a, respectively) is observed across the samples even within a single exposure, possibly indicating bulk chemistry variations within the litho-unit. **Clinopyroxene** is of two generations. Texturally early clinopyroxene (Cpx_1, $X_{Mg} \sim 0.57–0.77$) occurs either as porphyroblasts with marginal growth of hornblende (Fig. 4b), or is overgrown by garnet coronae (Fig. 4e). Late clinopyroxene (Cpx_2, $X_{Mg} \sim 0.57–0.80$) occurs in association with orthopyroxene along margins of hornblende that defines the S_{2JP} foliation, or along with second generation garnet (Grt_2) that has grown along the plagioclase–orthopyroxene interfaces (Fig. 4f). Cores of early clinopyroxene porphyroblasts (Cpx_1, viz. analyses points K280a-24, K280a-25, K280a-26, Table 2) that are mantled by garnet are relatively Fe-rich compared to the rims (viz. analyses points K280a-27, and K280a-28; Table 2), or with respect to the small clinopyroxene inclusions ($X_{Mg} \sim 0.77$, Table 2) in garnets (Grt_2). Clinopyroxene occurring along the margins of second generation garnet (Grt_2) viz. analyses points K280a-69, K280a-71, K280a-45, etc.; see Table 2) are interpreted to be products of the second granulite facies metamorphic event, but are now compositionally similar to texturally early clinopyroxene. **Orthopyroxene** is also inferred to be of two generations. The earlier generation orthopyroxene (Opx_1, Table 2) occurs as porphyroblasts that have retrogressed to biotite or are armoured by garnet (Grt_2) and clinopyroxene (Cpx_2) assemblages (Fig. 4f). Later orthopyroxene (Opx_2, Table 2) occurs in association with garnet (Grt_2) and clinopyroxene (Cpx_2) along hornblende–plagioclase interfaces (Fig. 4g), or along biotite margins, overprinting the S_{1JP}, S_{2JP} and S_{3JP} fabrics. There is no systematic difference in chemical composition among the two generations of orthopyroxene. However, while the X_{Mg} is consistent within individual samples, it is observed to vary between samples (0.41–0.61), again reflecting the differing bulk chemistry of the host rock (Table 2). **Amphibole** in the charnockite/enderbite/charno-enderbite is mostly ferro-pargasite or pargasite with high X_K values (0.32–0.67, Table 3). Reactant amphibole grains, trapped within ortho- and clino pyroxenes, show variation in composition from core to rim. Enrichment of Na, K, Fe^{2+}, Ti and Al^{tot}, and depletion of Si and Mg in rims relative to the cores (Table 3) is conspicuous. The general rimward enrichment in Ti, Al^{VI} and $(Na + K)_A$ suggests edenite and Ti-tschermakite/pargasite substitution, suggesting increasing temperature. However, no systematic variation is observed in amphiboles within the recrystallized mosaic as most are very small and have apparently equilibrated after peak metamorphism. Small amphibole inclusions in garnets are also X_{Mg}-rich, similar to the cores of larger amphiboles included within pyroxenes. **Biotite** proportion shows wide spatial variation, and shows three important modes of occurrence: as inclusions within garnet (Grt_2) or orthopyroxene (Opx_2), as isolated grains in the matrix, and as marginal grains on orthopyroxene (Opx_1) or garnet porphyroclasts (Grt_1). Biotite of all three textural modes is compositionally homogeneous (Table 3). **Garnet** in the charnockitic suite is either annealed into the S_{2JP} mosaic (Grt_1?), or occurs as porphyroblasts and coronal/marginal phases on clinopyroxene/orthopyroxene/hornblende/ilmenite. Porphyroblastic or coronal garnets (definitively Grt_2) contain an assortment of inclusion phases such as Bt, Opx, Pl, Hbl, Cpx, Ilm and Rt. The mineralogy of the included phases is conformable with the matrix mineralogy. Within the mylonitised S_{3JP} bands, a few garnet porphyroblasts or porphyroclasts are replaced by an assemblage of biotite + plagioclase + quartz. Compositional difference among the three modes of garnets is not pronounced. However, the garnet (Grt_2) overgrowing orthopyroxene (X_{Alm} 0.63–0.67, X_{Py} 0.12–0.15, $X_{Grs.}$ 0.14–0.17; Table 4) or ilmenite ($\sim X_{Alm}$ 0.66, X_{Py} 0.13, X_{Grs} 0.17, X_{Andra} 0.02–0.04; Table 4), is relatively more Fe-rich than the garnets overgrowing hornblende/biotite (X_{Alm} 0.53–0.56, X_{Py} 0.22–0.26, X_{Grs} 0.13–0.18, X_{Andra} 0.05; Table 4) or clinopyroxene (X_{Alm} 0.55–0.63, X_{Py} 0.15–0.25, X_{Grs} 0.14–0.18; Table 4). **K-feldspar** occurs in three modes—as porphyroclasts set within a fine-grained granoblastic mosaic, as marginal grains on biotite or garnet and as blebs in plagioclase; all texturally modes are chemically similar (Table 1). **Ilmenite** shows close association with hornblende and pyroxene. It occurs in three modes of occurrence – as matrix phase mantled by garnet, as inclusions within clinopyroxene, and as an exsolved phase along the margins or cleavages of hornblende. However, there is practically no difference in composition (X_{Fe} 0.95–0.99, X_{Mg} 0.04–0.00; Table 2) among the ilmenites of different modes.

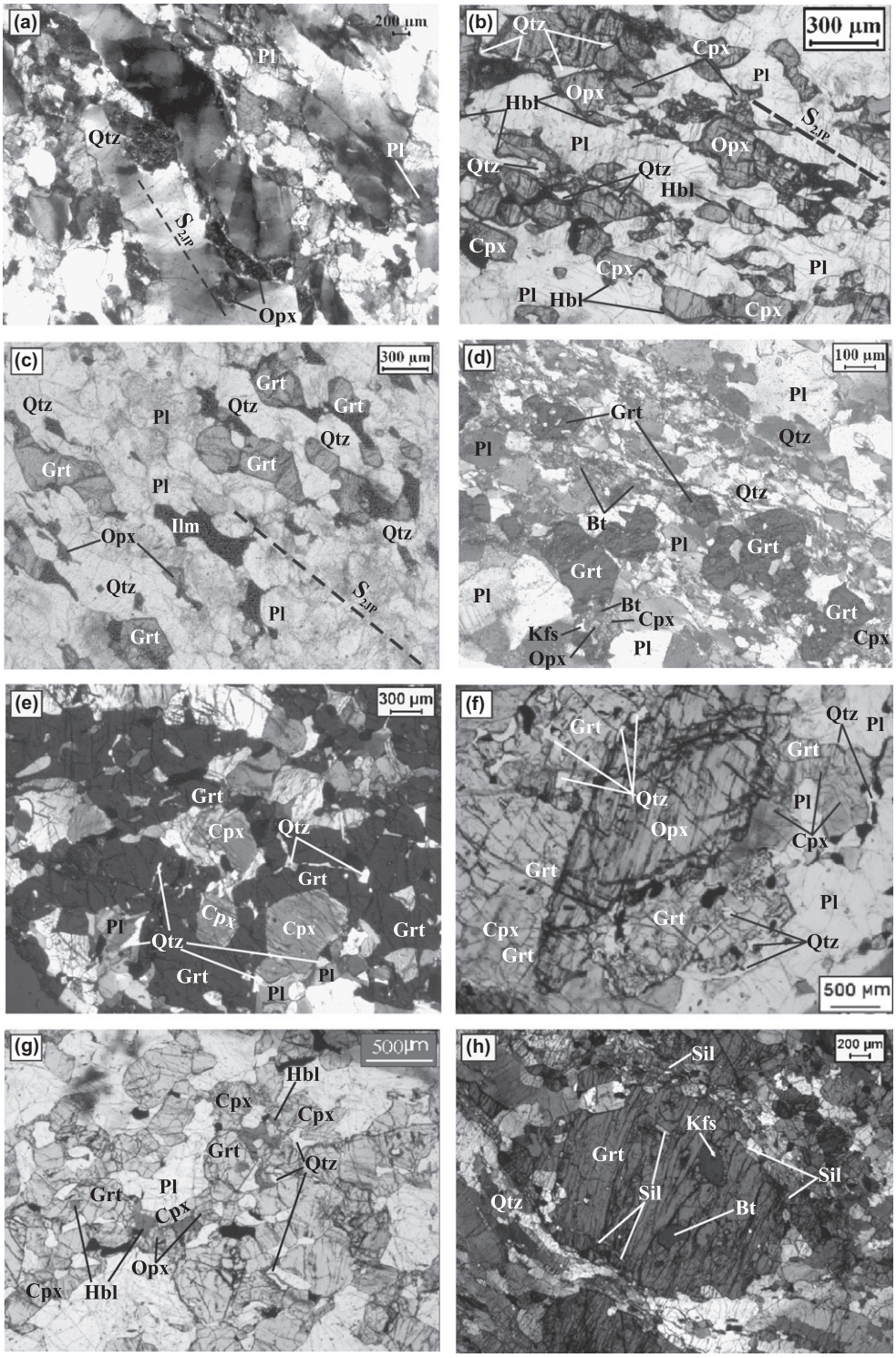

Fig. 4. Photomicrographs showing textural relationships in rocks of the study area. (a) Mylonitic S_{2JP} foliation in charnockitic rock of the Jeypore Province, characterized by ribbon/flattened Qtz with chessboard structures that imply high temperature deformation. (b) Pl and Opx show preferred alignment along the S_{2JP} foliation in charno-enderbite. (c) Grt annealed into the S_{2JP} fabric in charnockite along with Opx, Ilm, Pl, and Qtz. (d) Grt porphyroblasts overgrowing the S_{3JP} foliation in a shear band. (e) Texturally early clinopyroxene (Cpx_1) overgrown by Grt coronae intergrown with Qtz inclusions (photograph taken with partially crossed nicols). (f) Marginal growth of clinopyroxene (Cpx_2), garnet (Grt_2) and Qtz on orthopyroxene (Opx_1) porphyroclast in enderbites. Note that Qtz rims or wedges within the reaction domain are almost undeformed. (g) Late garnet (Grt_2), clinopyroxene (Cpx_2) and orthopyroxene (Opx_2) forming at the expense of hornblende along plagioclase interfaces in charno-enderbite. Note that Qtz wedges are undeformed. (h) Photomicrograph of Grt porphyroblast with Bt and Sil inclusions in garnet–sillimanite gneiss of the EGP (photograph taken with partially crossed nicols). Kfs occurs both as inclusion and matrix phase, and is inferred to be a product of this reaction.

Table 1
Representative chemical analyses of feldspars in enderbite and charno-enderbite of the JP and garnet–sillimanite gneisses of the EGP.

Plagioclase										K-feldspar		
Charnockite/charno-enderbite/enderbite										Charnockitic rock		G-Sil gneiss
Sample	K279-79	K279-47	K279-87	K280a-51	K280a-33	K280a-72	K280a-55	K286a-7	K280a-32	K286a-10	K286a-3	K281-34
Textural site	Matrix core	Matrix core	Rim of matrix	Near Grt_2 corona	Near Grt_2 corona	Near Grt_2 corona	Matrix	Matrix	Matrix	Porc. G_1	Mantling Bt	Near Bt incl in Grt_2
SiO_2	54.92	54.22	54.67	59.49	58.44	59.17	59.02	57.55	58.84	63.79	63.72	64.37
TiO_2	0.00	0.02	0.00	0.00	0.00	0.00	0.04	0.01	0.00	0.00	0.00	0.00
Al_2O_3	27.63	27.71	27.18	24.69	25.21	24.72	24.87	25.92	25.32	18.70	18.31	18.94
Cr_2O_3	0.01	0.00	0.00	0.00	0.00	0.00	0.01	0.04	0.00	0.02	0.05	0.00
Fe_2O_3	0.10	0.10	0.24	0.11	0.08	0.04	0.00	0.13	0.13	0.09	0.41	0.14
FeO	0.00	0.00	0.00	0.00	0.00	0.00	0.00	0.00	0.00	0.00	0.00	0.00
MnO	0.02	0.00	0.00	0.00	0.00	0.00	0.00	0.00	0.00	0.00	0.01	0.00
MgO	0.00	0.02	0.00	0.00	0.00	0.01	0.00	0.00	0.01	0.00	0.00	0.01
CaO	10.96	11.37	11.25	7.29	7.85	7.20	7.61	8.15	7.64	0.00	0.02	0.14
Na_2O	5.25	4.90	5.17	6.93	6.55	7.15	7.13	6.91	6.95	0.64	0.51	1.78
K_2O	0.14	0.16	0.13	0.33	0.32	0.30	0.33	0.15	0.29	15.76	15.86	13.72
Total	99.03	98.50	98.64	98.84	98.45	98.59	99.01	98.86	99.18	99.00	98.89	99.10
(O)	8	8	8	8	8	8	8	8	8	8	8	8
Si	2.500	2.484	2.502	2.681	2.649	2.675	2.662	2.606	2.649	2.976	2.981	2.976
Ti	0.000	0.001	0.000	0.000	0.000	0.000	0.001	0.000	0.000	0.000	0.000	0.000
Al	1.483	1.496	1.466	1.312	1.347	1.318	1.322	1.384	1.344	1.029	1.010	1.032
Cr^{3+}	0.000	0.000	0.000	0.000	0.000	0.000	0.000	0.001	0.000	0.001	0.002	0.000
Fe^{3+}	0.003	0.003	0.008	0.004	0.003	0.002	0.000	0.005	0.005	0.003	0.014	0.005
Fe^{2+}	0.000	0.000	0.000	0.000	0.000	0.000	0.000	0.000	0.000	0.000	0.000	0.000
Mn	0.001	0.000	0.000	0.000	0.000	0.000	0.000	0.000	0.000	0.000	0.000	0.000
Mg	0.000	0.001	0.000	0.000	0.000	0.001	0.000	0.000	0.001	0.000	0.000	0.001
Ca	0.535	0.558	0.552	0.352	0.381	0.349	0.368	0.395	0.368	0.000	0.001	0.007
Na	0.463	0.435	0.459	0.606	0.576	0.627	0.624	0.607	0.607	0.058	0.046	0.160
K	0.008	0.009	0.008	0.019	0.019	0.017	0.019	0.009	0.017	0.939	0.948	0.810
Sum	4.993	4.987	4.995	4.974	4.975	4.989	4.996	5.007	4.991	5.006	5.002	4.991
X_{Ca}	0.53	0.56	0.54	0.36	0.39	0.35	0.36	0.39	0.37	0.00	0.00	0.01
X_{Na}	0.46	0.43	0.45	0.62	0.59	0.63	0.62	0.60	0.61	0.06	0.05	0.16
X_K	0.01	0.01	0.01	0.02	0.02	0.02	0.02	0.01	0.02	0.94	0.95	0.83

Grt_1 = texturally early garnet, Grt_2 = texturally late garnet, porb. = porphyrobalst, incl = inclusion, porc. = porphyroclast.

5.2. Eastern Ghats Province

The quartzofeldspathic/feldspathic gneiss of this province occur as discontinuous bands within the dominantly metapelitic terrain, but is the most well preserved of the lithological units of the EGP within the study area. The rocks are composed of plagioclase, quartz, biotite, K-feldspar, orthopyroxene, garnet, ilmenite ± hornblende ± clinopyroxene. The accessories present are rutile, calcite and zircon. The gneissic appearance is imparted by alternately arranged leucocratic and melanocratic layers (S_{1EG}). The garnets are mostly coronal on orthopyroxene/ilmenite/biotite; these minerals within the S_{1EG} melanocratic layers imply that granulite facies conditions existed during D_{1EG}. S_{1EG} is truncated by and/or transposed along the S_{2EG} and S_{3EG} shear foliations (Gupta et al., 2005; Nanda and Gupta, 2008; Nanda et al., 2008). These two later foliations are defined by biotite and recrystallised aggregates of quartz and feldspar. The assemblage garnet ± orthopyroxene ± clinopyroxene in association with undeformed K-feldspar occurs along the margins of S_{2EG} and S_{3EG} biotite and therefore post-dates the D_{2EG} and D_{3EG} deformation events (Nanda et al., 2008). The mineral chemistry of the minerals of this lithological unit of EGP has been documented by Nanda et al. (2008) in detail. A summary of the compositions of the major phases is reproduced in Table 5.

In garnet–sillimanite bearing metapelites of the EGP the gneissic layering, S_{1EG}, is defined by segregation into quartzofeldspathic and biotite + sillimanite + garnet bearing layers. S_{2EG}, which is invariably parallel to S_{1EG}, is defined by aligned acicular sillimanite, ribbon quartz and platy K-feldspars and wraps around garnet porphyroblasts. Biotite shows wide variation in abundance. Though rarely present in the mosaic, biotite mostly occurs as inclusions within garnet porphyroblasts in sillimanite-rich domains. In sillimanite-poor domains, biotite defines the S_{2EG} foliation, and also occurs as inclusions in garnet porphyroblasts. The included trails (S_{1EG}?) of rounded to sub-rounded biotite are closely associated with K-feldspar inclusions. In places, the trails are at very high angles to the quartz ribbon and sillimanite defining the S_{2EG} foliation. Sphene and rutile occur as accessory phases and are present as inclusions in garnet or grown marginally on garnet. **Garnet** porphyroblasts are compositionally homogeneous (X_{Alm} 0.61–0.64, X_{Py} 0.31–0.34, X_{Andra} 0.00–0.05, Table 4) with inclusions of biotite, rutile, sillimanite, and **K-feldspar** (~X_K 0.83, X_{Na} 0.16, Table 1; Fig. 4 h). K-feldspar also occurs as porphyroblasts and is chemically similar to the inclusions in garnet. **Biotite** is almost erased from the matrix in sillimanite-rich domains. The biotite inclusions in garnets are Mg rich (~X_{Mg} 0.64, Table 3), while that in sillimanite-poor domains within the matrix is relatively iron rich (~X_{Mg} 0.58).

6. Reconstruction of metamorphic reactions and the P-T path

6.1. Jeypore Province

The mineral assemblage stable in the S_{1JP} fabric indicates that the accompanying deformation operated synchronous with granulite facies metamorphism. During D_{2JP} and D_{3JP} shearing, the $Opx_1 + Cpx_1 + Grt_1$ assemblage within the S_{1JP} foliation was

retrogressed to biotite and hornblende (Fig 4b). Following D_{3JP}, a second granulite facies assemblage (Opx_2 + Grt_2 + Kfs + Qtz ± Cpx_2) overprints all earlier foliations. $Opx_2 \pm Cpx_2$ grew marginally on biotite or hornblende via the reactions

$$Bt + Qtz \rightarrow Opx + Kfs + H_2O, \quad (R1)$$

and

$$Hbl \rightarrow Opx + Cpx + Qtz + H_2O. \quad (R2)$$

In places, hornblende was erased from the assemblage by reaction R2. The second generation porphyroblastic garnet (Grt_2) and clinopyroxene (Cpx_2; Fig. 4d) formed by the reaction

$$Bt + Pl + Opx \rightarrow Grt + Cpx + Kfs + H_2O. \quad (R3)$$

Garnet coronae also grew along with quartz following Cpx-Pl interfaces (Fig. 4e) via the reaction

$$Cpx + Pl \rightarrow Grt + Qtz, \quad (R4)$$

and along Opx-Pl interfaces by the reaction

$$Opx + Pl \rightarrow Grt + Qtz. \quad (R5)$$

The reaction

$$Opx + Pl \rightarrow Grt + Cpx + Qtz \quad (R6)$$

produced garnet + clinopyroxene, with very thin rims of quartz on orthopyroxene porphyroclasts (Fig. 4f).

Production of Grt_2 and Cpx_2 porphyroblasts that contain hornblende inclusions (Fig. 4g) can be modelled by the reaction

$$Hbl + Pl \rightarrow Grt + Cpx + Qtz + H_2O. \quad (R7)$$

In places where Cpx is absent, Grt_2 + Qtz formed by the reaction

$$Hbl + Pl \rightarrow Grt + Qtz + H_2O. \quad (R8)$$

The chemographic projections in support of the metamorphic reactions R3, R5 and R7 are given in Fig. 5a and b.

6.2. Eastern Ghats Province

In garnet–sillimanite gneiss, garnet porphyroblasts (X_{Fe} 0.61–0.64, X_{Mg} 0.31–0.34, Table 4) in association with K-feldspar, sillimanite and biotite appear to have formed by the reaction

$$Bt + Qtz + Sill \rightarrow Grt + Kfs + H_2O. \quad (R9)$$

Plagioclase was erased from garnetiferous domain via the reaction

$$Bt + Qtz + Pl \rightarrow Grt + Kfs + H_2O. \quad (R10)$$

The modelled metamorphic reactions that stabilized the second generation granulite facies assemblages in the charnockites, charno-enderbites and enderbites of the Jeypore Province are shown in Fig. 6. The reactions were plotted with the program THERMOCALC (v. 3.21) using the observed activities of corresponding mineral phases. Mg end-members have been used for plotting the reactions; similar constructions have also been made with the Fe-end-members. The reactions have been plotted only to show the sense in which they were crossed (shown by dark gray arrows, Fig. 6), as inferred from reaction textures, during the second granulite event.Reactions R2 and R7 indicate heating, while reactions R4, R5, R6 and R8 are compatible with loading. In domains where hornblende was erased via reaction R2, garnet stabilized on the anhydrous assemblage by reaction R4, R5 and R6. Garnet growth along hornblende–plagioclase interfaces occurred through reactions R7 and R8. Thus, the sequence of reaction textures is best explained by a heating followed by loading trajectory (light gray arrow, Fig. 6). A similar trajectory is derived if Fe-end-member reactions are plotted. Importantly, the inferred path is consistent with that established earlier by Nanda et al. (2008) from feldspathic/quartzofeldspathic gneisses in the adjacent EGP.

7. Thermobarometry

The sequence of mineral reactions in the enderbites and charnoenderbites of Jeypore province indicates that the first granulite facies metamorphic event (M_{1JP}) was followed by hydrous fluid infiltration and retrogression. This was succeeded by progressive dehydration with heating followed or accompanied by loading, culminating in a second granulite facies metamorphic event, M_{2JP}. Estimation of metamorphic conditions for the M_{1JP} event is not possible, as phases identified to be texturally early (e.g. garnet, clinopyroxene and orthopyroxene) are compositionally indistinguishable from the corresponding phases that are texturally late (i.e. syn-M_{2JP}). This indicates that potential M_{1JP} mineral assemblages amenable to thermobarometric analysis have almost completely re-equilibrated during the later M_{2JP} event. Consequently, all pressures and temperatures estimated in this study are essentially documents of the later M_{2JP} metamorphic event, irrespective of their textural locale, and the existence of an early M_{1JP} event is only inferred from the textural record.

Peak temperatures attained during the second granulite event (M_{2JP}) have been estimated using a combination of conventional geothermometers—garnet–clinopyroxene (Ellis and Green, 1979; Powell, 1985; Krogh, 1988; Ganguly et al., 1996), garnet–orthopyroxene (Harley, 1984; Ganguly et al., 1996), garnet–amphibole (Graham and Powell, 1984), and garnet–biotite (Ferry and Spear, 1978; Dasgupta et al., 1991). Representative temperature estimates are given in Table 6. As can be seen from the results obtained, the temperature estimates vary widely depending on the formulation used for calculation. A general observation is that the range of temperature estimates derived using various Grt–Cpx thermometers (603–784 °C, at 8 kb pressure) are consistent (see Table 6) with the estimates derived using the Grt–Hbl thermometer (614–730 °C), Grt–Opx thermometers (607–786 °C, at 8 kb pressure) and the Grt–Bt thermometers (725–807 °C, at 8 kb). More importantly, temperatures retrieved using compositions of the cores of garnet coronae or porphyroblasts, and clinopyroxene inclusions within these garnets or cores of the clinopyroxene porphyroblasts in the matrix, are relatively higher (~100 °C) than rim–rim pairs (see Grt–Cpx and Grt–Opx pairs in Table 6); this may be the result of post-peak (M_{2JP}) re-equilibration (e.g., Dodson, 1973) between the marginal part of the garnet and the adjacent pyroxene. The highest temperatures, obtained using compositions of the middle of garnet coronae along with core compositions of clinopyroxene and orthopyroxene grains rimmed by the garnet, are comparable (784 °C and 778 °C, respectively). The maximum temperature is obtained from garnet–biotite thermometry, using core compositions of garnet porphyroblasts in conjunction with biotite inclusions (807 °C). Therefore, peak temperatures attained during the second granulite facies metamorphic event (M_{2JP}) are estimated to have been ~800 °C.

Peak pressures reached during the second granulite facies (M_{2JP}) metamorphic event have also been constrained using conventional geobarometers (Newton and Perkins, 1982; Moecher et al., 1988; and Kohn and Spear, 1990; see Table 6 for details) and the average P-T mode incorporated in THERMOCALC (v. 3.21). Though retrieved pressures range from 5.8 kb to 8.6 kb, the preferred estimates are around ~8.0 ± 0.5 kb, the values obtained with the Fe-end members calibrated thermometers, as the bulk mineralogy of the studied samples is iron rich (see the GAFS, GAHS and P_{Fe} data sets in Table 6). Average PT results (7.6–8.7 kb, ~765 °C, Table 7) derived using THERMOCALC are also consistent with these values.

Table 2
Representative chemical analyses of clinopyroxene, orthopyroxene and ilmenite in charnockite, charno-enderbite and enderbite of the JP.

Clinopyroxene

Sample	K280a-24	K280a-25	K280a-26	K280a-27	K280a-28	K280a-71	K280a-69	K280a-45	K279-72	K279-75	K286a-31	K286a-11
Textural site	CoreCpx_1	Core Cpx_1	Core Cpx_1	Rim Cpx_1	Rim Cpx_1	Rim Cpx_2	Rim Cpx_2	Rim Cpx_2	Incl in Grt_2 corona	Incl in Grt_2 corona	Rim Cpx_2	Rim Cpx_2
SiO_2	51.17	50.98	50.81	50.55	51.40	50.62	50.70	51.25	50.49	50.45	51.50	52.01
TiO_2	0.18	0.27	0.21	0.14	0.08	0.18	0.23	0.13	0.28	0.44	0.15	0.13
Al_2O_3	1.55	1.79	1.64	1.26	1.25	1.65	1.57	1.34	3.04	3.44	1.74	1.78
Cr_2O_3	0.04	0.03	0.05	0.00	0.05	0.01	0.01	0.00	0.00	0.01	0.04	0.01
Fe_2O_3	1.17	2.09	2.58	3.40	1.70	1.02	1.60	1.39	3.32	2.79	2.80	2.48
FeO	14.87	11.48	11.33	9.64	10.82	13.25	13.69	11.69	8.09	6.55	5.80	7.15
MnO	0.22	0.15	0.17	0.14	0.14	0.10	0.16	0.05	0.13	0.05	0.14	0.07
MgO	11.08	10.72	10.60	11.84	11.67	9.95	10.27	10.91	14.20	12.39	13.33	13.33
CaO	19.05	22.02	21.80	21.65	21.72	21.84	20.90	22.03	19.45	22.80	22.84	22.31
Na_2O	0.44	0.48	0.54	0.42	0.42	0.35	0.41	0.43	0.47	0.61	0.58	0.58
K_2O	0.02	0.01	0.04	0.00	0.00	0.00	0.00	0.00	0.00	0.00	0.02	0.02
Total	99.79	100.02	99.77	99.04	99.25	98.97	99.54	99.22	99.47	99.53	98.94	99.87
(O)	6	6	6	6	6	6	6	6	6	6	6	6
Si	1.959	1.940	1.940	1.934	1.960	1.955	1.950	1.962	1.895	1.894	1.939	1.944
Ti	0.005	0.008	0.006	0.004	0.002	0.005	0.007	0.004	0.008	0.012	0.004	0.004
Al	0.070	0.080	0.074	0.057	0.056	0.075	0.071	0.060	0.135	0.152	0.077	0.078
Cr^{3+}	0.001	0.001	0.002	0.000	0.002	0.000	0.000	0.000	0.000	0.000	0.001	0.000
Fe^{3+}	0.034	0.060	0.074	0.098	0.049	0.030	0.046	0.040	0.094	0.079	0.079	0.070
Fe^{2+}	0.476	0.365	0.362	0.309	0.345	0.428	0.440	0.374	0.254	0.206	0.183	0.223
Mn	0.007	0.005	0.005	0.005	0.005	0.003	0.005	0.002	0.004	0.002	0.004	0.002
Mg	0.632	0.608	0.603	0.675	0.663	0.573	0.589	0.622	0.794	0.693	0.748	0.742
Ca	0.782	0.898	0.892	0.888	0.887	0.904	0.861	0.904	0.782	0.917	0.921	0.893
Na	0.033	0.035	0.040	0.031	0.031	0.026	0.031	0.032	0.034	0.044	0.042	0.042
K	0.001	0.000	0.002	0.000	0.000	0.000	0.000	0.000	0.000	0.000	0.001	0.001
Sum	4.000	4.000	4.000	4.001	4.000	3.999	4.000	4.000	4.000	3.999	3.999	3.999
X_{Mg}	0.57	0.62	0.62	0.69	0.66	0.57	0.57	0.62	0.76	0.77	0.80	0.77
Al^T	0.041	0.06	0.06	0.057	0.04	0.045	0.05	0.038	0.105	0.106	0.061	0.056

Orthopyroxene

Sample	K280a114	K279–60	K280a-64	K280a65	K280a-66	K280a-37	K280a-39	K286a-15
Textural site	Core Opx_1	Core Opx_2	Core Opx_2	Rim Opx_2	Rim Opx_2	Core Opx_2	Rim Opx_2	Matrix Opx_2
SiO_2	50.67	51.19	49.45	49.26	49.69	50.39	50.76	51.36
TiO_2	0.05	0.04	0.09	0.07	0.09	0.02	0.07	0.06
Al_2O_3	0.65	2.01	0.79	0.90	0.48	0.44	0.53	1.25
Cr_2O_3	0.00	0.00	0.03	0.02	0.00	0.00	0.00	0.03
Fe_2O_3	0.23	1.32	0.00	2.06	0.56	0.89	0.00	1.56
FeO	35.19	23.48	33.66	27.00	32.75	32.72	31.28	24.71
MnO	0.25	0.31	0.38	0.24	0.28	0.34	0.23	0.23
MgO	13.50	20.64	13.44	13.13	14.36	14.83	15.09	20.13
CaO	0.64	0.52	0.80	6.10	0.66	0.46	0.54	0.33
Na_2O	0.06	0.00	0.00	0.11	0.00	0.04	0.03	0.05
K_2O	0.01	0.00	0.00	0.00	0.01	0.00	0.03	0.00
Total	101.25	99.51	98.64	98.89	98.88	100.13	98.56	99.71
(O)	6	6	6	6	6	6	6	6
Si	1.983	1.935	1.980	1.950	1.978	1.978	2.003	1.949
Ti	0.001	0.001	0.003	0.002	0.003	0.001	0.002	0.002
Al	0.030	0.090	0.037	0.042	0.023	0.020	0.025	0.056
Cr^{3+}	0.000	0.000	0.001	0.001	0.000	0.000	0.000	0.001
Fe^{3+}	0.007	0.038	0.000	0.061	0.017	0.026	0.000	0.045
Fe^{2+}	1.152	0.743	1.127	0.894	1.090	1.074	1.032	0.784

Ilmenite

Sample	K279-50	K280a-54	K280a-92	K280a-91
	Incl in Cpx	Incl in Grt corona	Core, mant. Grt corona	Rim, mant. Grt corona
SiO_2	0.03	0.00	0.00	0.00
TiO_2	45.46	52.27	51.35	51.71
Al_2O_3	0.02	0.00	0.02	0.00
Cr_2O_3	0.02	0.00	0.05	0.01
Fe_2O_3	13.15	0.39	1.81	0.94
FeO	38.75	46.31	44.68	46.13
MnO	0.25	0.35	0.24	0.15
MgO	0.96	0.07	0.60	0.11
CaO	0.01	0.00	0.05	0.02
Na_2O	0.02	0.02	0.00	0.00
K_2O	0.03	0.04	0.04	0.00
Total	98.70	99.45	98.84	99.07
(O)	3	3	3	3
Si	0.001	0.000	0.000	0.000
Ti	0.873	0.997	0.982	0.991
Al	0.001	0.000	0.001	0.000
Cr^{3+}	0.000	0.000	0.001	0.000
Fe^{3+}	0.253	0.007	0.035	0.018
Fe^{2+}	0.828	0.983	0.951	0.983

Mn	0.008	0.010	0.013	0.008	0.009	0.011	0.008	0.007	Mn	0.005	0.008	0.005	0.003	
Mg	0.787	1.163	0.802	0.775	0.852	0.867	0.888	1.139	Mg	0.037	0.003	0.023	0.004	
Ca	0.027	0.021	0.034	0.259	0.028	0.019	0.023	0.013	Ca	0.000	0.000	0.001	0.001	
Na	0.005	0.000	0.000	0.008	0.000	0.003	0.002	0.004	Na	0.001	0.001	0.000	0.000	
K	0.000	0.000	0.000	0.000	0.001	0.000	0.002	0.000	K	0.001	0.001	0.001	0.000	
Sum	4.000	4.001	3.997	4.000	4.001	3.999	3.985	4.000	Sum	2.000	2.000	2.000	2.000	
X_{Mg}	0.41	0.61	0.42	0.46	0.44	0.45	0.46	0.59	X_{Fe}	0.95	0.99	0.97	0.99	
Al^T	0.017	0.065	0.02	0.042	0.022	0.020	0.000	0.051	X_{Mn}	0.01	0.01	0.01	0.00	

Grt_2 = second generation garnet, incl = inclusion, Cpx_1 = clinopyroxene of earlier granulite event, Cpx_2 = clinopyroxene of later granulite event, Opx_1 = orthopyroxene of earlier generation, Opx_2 i = orthopyroxene of later generation. Core, mant. = core of the grain mantled by, rim, mant. = rim of the grain mantled by.

The peak metamorphic pressure–temperature condition estimated by Nanda et al. (2008) from the adjacent feldspathic/quartzofeldspathic and alkaline rocks of the EGP for the second granulite facies metamorphic event are slightly lower, but generally in agreement with the present estimates from the rocks of the Jeypore Province–EGP contact zone made in this study.

8. Schreinemakers construction and sense of the P-T path

The sense of the P-T trajectory followed during the second granulite facies metamorphic event can be confirmed from a Schreinemakers construction around an invariant point in a five component CFASH or CMASH system, involving the seven phases hornblende, orthopyroxene, clinopyroxene, garnet, plagioclase, quartz and water (in fluid). The selected system is appropriate for representing the documented textural reactions in the enderbites and charnockites, with anorthite (plagioclase), quartz and fluid considered to be in excess. Invariant points can be separately calculated for the pure end-member CFASH (2.9 kb, 353 °C) and CMASH (12.1 kb, 668 °C) systems, and the Schreinemakers constructions in both cases have similar topologies, although the locations of the respective invariant points in P-T space merely serve to bracket the locations of the associated reactions for the intermediate CFMASH system. Similar constructions using activities calculated from measured compositions of the mineral phases (i.e. activity-corrected) also produce similar topologies. For these cases, the invariant point positions in P-T space for the CFASH and CMASH systems are (7.7 kb, 786 °C) and (8.1 kb, 707 °C) respectively, at $a_{H_2O} = 0.1$. Although the end-member systems are useful for depicting the sequence in which reactions were crossed, it must be kept in mind that all the univariant reactions shown are essentially divariant (continuous) in the CFMASH system. Nevertheless, these constructions serve to illustrate that the observed textural sequence can only be explained by a heating followed or accompanied by loading trajectory.

Although 'activity corrected' diagrams are useful for validating the P-T trajectory that explains the observed textural sequence, these are only valid at conditions close to the pseudo-invariants defined by buffering assemblages and the given component activities (Fitzsimons and Harley, 1995). Moreover, such grids do not consider changes in component activities that occur as reactions progress and mineral compositions adjust to those changes in conditions. In the present case, the stability fields of hornblende and orthopyroxene are expected to expand as a consequence of Tschermak substitution, and this may change the topology of the grid with changing P-T conditions. Keeping these in mind, the invariant point shown in Fig. 7 has been calculated using THERMOCALC v. 3.26 for the CMASH system, as the THERMOCALC database includes thermodynamic information for the appropriate Al-bearing components in the Mg end-member system (but not the Fe end-member system) that take into account the solubility of Al into the amphibole and orthopyroxene structure. In the calculation, the asymmetric formalism model was used for hornblende solid solution (comprising tremolite and tschermakite), while symmetric mixing models were adopted for orthopyroxene (enstatite and the Mg-Tschermak molecule) and garnet (pyrope and grossular); diopside (clinopyroxene), anorthite (plagioclase) and quartz were considered to be pure phases. Details of the models used are provided as a Supplementary Item. Water activity for the fluid phase was assumed to be 0.1, as constrained from the overlap between P-T values calculated using hydrous and anhydrous phases (e.g. Nanda et al., 2008). As can be observed from Fig. 7, the breakdown of hornblende by the (g) reaction necessarily implies increasing temperature; any surviving hornblende would react with plagioclase to form garnet–clinopyroxene–quartz by the metastable

Table 3
Representative chemical analyses of **amphibole** and **biotite** from the charnockitic rocks of the JP and garnet–sillimanite gneiss of the EGP.

Amphibole

Charnockite/charno-enderbite/enderbite

Sample	K279-37	K279-39	K279-38	K279-40	K280a-111	K280a-108	K280a-112	K280a-86	K280a-87	K279-96	K279-81	K279-73
Tex. site	Core incl in Cpx	Rim incl in Cpx	Core incl in Cpx	Rim incl in Cpx	Matrix	Matrix	Matrix	Matrix	Matrix	Incl in Grt_2	Incl in Grt_2	Incl in Grt_2
SiO_2	42.65	41.20	43.50	41.26	42.51	40.07	40.95	39.75	40.09	42.09	42.65	43.84
TiO_2	1.89	2.02	1.92	2.17	2.05	1.93	1.55	0.20	2.28	2.18	2.33	0.57
Al_2O_3	11.53	12.44	11.16	12.56	11.18	12.52	12.41	15.68	12.53	12.16	11.76	11.40
Cr_2O_3	0.06	0.10	0.00	0.06	0.09	0.00	0.04	0.03	0.07	0.00	0.03	0.00
Fe_2O_3	1.66	1.34	1.52	0.93	0.23	0.13	0.44	2.21	0.38	2.79	0.84	4.88
FeO	12.86	13.30	13.03	14.31	19.51	19.21	19.45	16.59	19.03	9.98	11.93	7.94
MnO	0.02	0.06	0.07	0.08	0.07	0.06	0.07	0.00	0.08	0.06	0.05	0.00
MgO	11.50	10.91	11.51	10.34	7.80	7.45	7.49	7.02	7.25	12.96	12.44	13.91
CaO	11.64	11.76	11.58	11.78	11.62	11.88	11.83	11.51	11.44	11.58	12.05	12.47
Na_2O	1.62	1.72	1.57	1.71	1.29	1.25	1.25	0.84	1.26	1.92	1.79	1.30
K_2O	1.00	1.23	0.93	1.21	1.88	2.14	2.21	2.03	2.20	0.88	1.05	0.94
Total	96.43	96.08	96.79	96.41	98.23	96.64	97.69	95.86	96.61	96.6	96.92	97.25
(O)	23	23	23	23	23	23	23	23	23	23	23	23
Si	6.408	6.252	6.498	6.259	6.469	6.233	6.299	6.142	6.232	6.259	6.351	6.431
Ti	0.214	0.231	0.216	0.248	0.235	0.226	0.179	0.023	0.267	0.244	0.261	0.063
Al	2.042	2.226	1.965	2.246	2.006	2.296	2.251	2.857	2.296	2.132	2.064	1.971
Cr^{3+}	0.007	0.012	0.000	0.007	0.011	0.000	0.005	0.004	0.009	0.000	0.004	0.000
Fe^{3+}	0.188	0.153	0.170	0.106	0.027	0.016	0.051	0.257	0.045	0.313	0.094	0.538
Fe^{2+}	1.617	1.688	1.627	1.816	2.483	2.499	2.503	2.144	2.474	1.241	1.486	0.974
Mn	0.003	0.008	0.009	0.010	0.009	0.008	0.009	0.000	0.011	0.008	0.006	0.000
Mg	2.575	2.467	2.562	2.338	1.769	1.727	1.717	1.617	1.680	2.872	2.761	3.041
Ca	1.874	1.912	1.854	1.915	1.895	1.980	1.950	1.906	1.906	1.845	1.923	1.960
Na	0.472	0.506	0.455	0.503	0.381	0.377	0.373	0.252	0.380	0.554	0.517	0.370
K	0.192	0.238	0.177	0.234	0.365	0.425	0.434	0.401	0.437	0.167	0.200	0.176
Sum	15.592	15.693	15.533	15.682	15.650	15.787	15.771	15.603	15.737	15.635	15.667	15.524
Na_B	0.07	0.05	0.10	0.05	0.10	0.02	0.04	0.05	0.08	0.09	0.05	0.02
Na_A	0.40	0.46	0.36	0.45	0.29	0.36	0.34	0.20	0.30	0.47	0.47	0.35
Al^T	1.59	1.75	1.50	1.74	1.53	1.77	1.70	1.86	1.77	1.74	1.65	1.57
Al^M	0.45	0.48	0.46	0.51	0.48	0.53	0.55	1.00	0.53	0.39	0.42	0.40
X_K	0.32	0.34	0.33	0.34	0.56	0.54	0.56	0.67	0.59	0.26	0.30	0.33
X_{Mg}	0.61	0.59	0.61	0.56	0.42	0.41	0.41	0.43	0.40	0.70	0.65	0.76

Biotite

Charnockite/charno-enderbite/enderbite					Grt–Sil gneiss	
Sample	K286a-17	K286a-2	K286a-1	K286a-30	K22-1	K281-38
Textural site	Matrix	Incl in Grt_2	Incl in Grt_2	Incl in Grt_2	Matrix	Incl in Grt_2
SiO_2	36.38	35.91	35.41	36.29	38.15	36.34
TiO_2	5.44	6.21	5.84	5.77	6.51	5.14
Al_2O_3	13.79	14.04	14.05	13.77	13.11	15.78
Cr_2O_3	0.13	0.00	0.08	0.07	0.00	0.06
Fe_2O_3	0.00	0.00	0.00	0.00	0.00	0.00
FeO	15.27	16.29	15.97	15.04	15.76	13.85
MnO	0.00	0.00	0.06	0.02	0.04	0.00
MgO	13.71	12.76	13.02	13.57	12.57	13.95
CaO	0.00	0.00	0.00	0.00	0.00	0.05
Na_2O	0.02	0.02	0.07	0.09	0.00	0.24
K_2O	9.74	9.76	10.01	9.79	9.87	9.65
Total	94.48	94.99	94.51	94.41	96.01	95.06

(O)	11	11	11	11	11	11
Si	2.761	2.726	2.708	2.756	2.845	2.715
Ti	0.311	0.355	0.336	0.330	0.365	0.289
Al	1.234	1.257	1.267	1.233	1.152	1.390
Cr^{3+}	0.008	0.000	0.005	0.004	0.000	0.004
Fe^{3+}	0.000	0.000	0.000	0.000	0.000	0.000
Fe^{2+}	0.969	1.034	1.022	0.955	0.983	0.866
Mn	0.000	0.000	0.004	0.001	0.003	0.000
Mg	1.551	1.444	1.484	1.536	1.397	1.554
Ca	0.000	0.000	0.000	0.000	0.000	0.004
Na	0.003	0.003	0.010	0.013	0.000	0.035
K	0.944	0.946	0.978	0.949	0.940	0.921
Sum	7.781	7.765	7.814	7.777	7.685	7.778
X_{Mg}	0.62	0.58	0.59	0.62	0.58	0.64

G_2 = second generation garnet, Cp = clinopyroxene, incl = inclusion, Grt–Sil = Garnet sillimanite.

extension of the (opx) reaction. Production of garnet, clinopyroxene and quartz from orthopyroxene and plagioclase by the (hb) reaction can only be explained by subsequent increase in pressure. It is emphasized once again that since the Fe-end members of the constituent phases have not been considered in the construction, the derived path is important more in a qualitative than a quantitative sense. A heating followed by loading, or heating associated with loading trajectory can explain the observed sequence of reaction textures in the enderbites and charno-enderbites of the Jeypore Province.

9. Discussion

9.1. Implications for the metamorphic evolution of the Jeypore Province

Integration of the structural and metamorphic information collated from this study has important implications for understanding the nature of the contact between the EGP and the Jeypore Province. Structurally, it has been demonstrated in this study that the easternmost part of the Jeypore Province and westernmost fringe of the adjoining EGP are both strongly sheared. The penetrative shear fabric in the charnockite suite of the Jeypore Province, S_{2JP}, is concordant with the S_{2EG} shear foliation in the EGP. Therefore, the D_{2JP} and D_{2EG} deformation events can be considered correlatable and coeval in both the provinces across the contact, and are henceforth collectively referred to as the D_2 event. The shear sense during this event suggests west-vergent thrusting, and indicates that the D_2 deformation was either associated with, or post-dates, amalgamation of the two provinces. The subsequent D_{3JP} and D_{3EG} events can likewise also be considered correlatable, and regarded as a single D_3 deformation event that affected both the provinces.

The results of this study also indicate that the eastern margin of the Jeypore Province which is adjacent to the EGP is polymetamorphic in character, having suffered at least two granulite facies events. An early granulite facies event, M_{1JP}, precedes the D_2 deformation and is indicated by the presence of texturally early clinopyroxene and orthopyroxene in the charnockite suite of rocks. Compositionally, however, these early pyroxenes are indistinguishable from the later pyroxenes that grew at the expense of hornblende and biotite. Loss of compositional identity of these texturally early (M_{1JP}) phases is easily explained as a consequence of overprinting and re-equilibration during the later M_{2JP} granulite event in the rocks of Jeypore Province. Estimates of metamorphic conditions during this early event were obtained from the western margin of the belt (5.5–5.6 kb, 640–780 °C, Subbarao et al., 1998). Since the last thermal event in this western boundary region occurred around 2.8 Ga (Kovach et al., 2001), this Archean age may be considered to correspond to M_{1JP} metamorphism. The metamorphic conditions and timing of the M_{1JP} event contrast sharply with the Grenvillian age (1.1–0.9 Ga) ultrahigh to high temperature metamorphism that constitutes the first identifiable metamorphic event (M_{1EG}) in the adjoining EGP (Dasgupta and Sengupta, 2003).

The sequence of metamorphic mineral growth in the eastern marginal part of the Jeypore Province investigated in this study suggests that hydrated assemblages formed during a retrogressive phase that followed early M_{1JP} metamorphism, and that the eastern boundary zone of the province subsequently underwent a second phase of granulite facies metamorphism (M_{2JP}). Since the granulite facies mineralogy overprints both S_{2JP} and S_{3JP} fabrics, the M_{2JP} event post-dates D_{2JP} and D_{3JP} deformation. This later metamorphic episode is characterized by a counter-clockwise prograde P-T trajectory (Figs. 6 and 7) identical to that preserved in the adjacent quartzofeldspathic/feldspathic gneisses of the adjoining EGP. Further to the east, in the Koraput area of the EGP, Nanda

Table 4
Representative analyses of **garnet** in rocks of EGP and JP.

Grt–Sil gneiss				Charnockite/charno-enderbite/enderbite							
Sample	K281-1	K281-19	K281-39	K280a-29	K280a30	K280a-40	K280a-44	K280a-67	K280a-93	K279-71	K279-70
Textural site	Rim porb.	Core porb.	Near bt incl	Grt_2 cor on Cpx	Grt_2 cor on Cpx	Grt_2 cor on Cpx	Grt_2 cor on Opx	Grt_2 cor on Opx	Grt_2 cor on Ilm	Grt_2 cor on Cpx	Grt_2 cor on Opx
SiO_2	37.94	38.26	38.04	37.56	37.49	37.55	36.88	37.79	37.18	38.33	38.95
TiO_2	0.02	0.07	0.01	0.10	0.00	0.03	0.00	0.06	0.22	0.00	0.00
Al_2O_3	21.87	21.39	21.56	20.95	21.27	20.80	20.91	20.47	20.58	21.01	21.45
Cr_2O_3	0.05	0.01	0.00	0.02	0.06	0.00	0.09	0.00	0.02	0.00	0.02
Fe_2O_3	2.32	0.85	1.71	2.33	2.09	2.23	1.94	1.16	1.46	1.50	0.31
FeO	27.55	29.25	27.40	27.80	28.22	28.61	29.29	29.21	29.25	25.02	25.40
MnO	0.20	0.23	0.23	0.77	0.77	0.79	0.68	0.73	0.73	0.92	0.71
MgO	8.71	8.05	8.59	3.89	3.74	3.32	2.99	3.46	3.03	6.45	6.63
CaO	1.59	1.52	1.70	7.21	6.96	7.26	6.75	7.10	7.16	6.51	6.74
Na_2O	0.01	0.00	0.08	0.04	0.04	0.05	0.03	0.00	0.02	0.01	0.00
K_2O	0.01	0.01	0.00	0.02	0.02	0.02	0.00	0.01	0.00	0.00	0.00
Total	100.27	99.64	99.32	100.69	100.66	100.66	99.56	99.99	99.65	99.75	100.21
(O)	12	12	12	12	12	12	12	12	12	12.000	12.000
Si	2.934	2.987	2.965	2.956	2.953	2.968	2.954	3.003	2.974	2.99	3.012
Ti	0.001	0.004	0.001	0.006	0.000	0.002	0.000	0.004	0.013	0	0.000
Al	1.994	1.969	1.981	1.944	1.975	1.938	1.974	1.918	1.940	1.932	1.956
Cr^{3+}	0.003	0.001	0.000	0.001	0.004	0.000	0.006	0.000	0.001	0	0.001
Fe^{3+}	0.135	0.050	0.100	0.138	0.124	0.133	0.117	0.069	0.088	0.088	0.018
Fe^{2+}	1.782	1.910	1.786	1.830	1.859	1.891	1.962	1.941	1.956	1.632	1.643
Mn	0.013	0.015	0.015	0.051	0.051	0.053	0.046	0.049	0.049	0.061	0.047
Mg	1.004	0.937	0.998	0.456	0.439	0.391	0.357	0.410	0.361	0.75	0.764
Ca	0.132	0.127	0.142	0.608	0.587	0.615	0.579	0.605	0.614	0.544	0.559
Na	0.001	0.000	0.012	0.006	0.006	0.008	0.005	0.000	0.003	0.002	0.000
K	0.001	0.001	0.000	0.002	0.002	0.002	0.000	0.001	0.000	0	0.000
Sum	8.000	8.001	8.000	7.998	8.000	8.001	8.000	8.000	7.999	7.999	8.000
X_{Grs}	0.05	0.02	0.00	0.14	0.14	0.14	0.14	0.17	0.16	0.14	0.18
X_{Alm}	0.61	0.64	0.61	0.62	0.63	0.64	0.67	0.65	0.66	0.55	0.55
X_{Py}	0.34	0.31	0.34	0.15	0.15	0.13	0.12	0.14	0.12	0.25	0.25
X_{Sps}	0.00	0.01	0.00	0.02	0.02	0.02	0.02	0.02	0.02	0.02	0.02
X_{Adr}	0.00	0.02	0.05	0.07	0.06	0.07	0.05	0.02	0.04	0.04	0.00
Al^T	0.13	0.03	0.07	0.09	0.09	0.06	0.09	0.00	0.05	0.02	0.00

Charnockite/enderbite/charno-enderbite										
Sample	K280a-68	K286a35	K279-84	K279-98	K286a-34	K280a-119	K279-82	K286a-4	K286a-6	K286a-110
Textural site	Grt_2 cor on Opx	Grt_2 cor on Bt	Cor near amp incl	Grt_2 porb. core	Grt_2 cor on Bt	Grt_2 Porb. rim	Grt_2 Porb. rim	core, near bt incl	Grt_2 porb. core	Grt_1 porc. core
SiO_2	37.04	37.78	38.28	38.57	38.18	37.87	37.96	37.88	38.20	38.00
TiO_2	0.00	0.02	0.06	0.06	0.03	0.04	0.11	0.00	0.02	0.04
Al_2O_3	20.24	21.48	21.00	20.82	21.20	20.93	20.55	21.45	21.29	21.48
Cr_2O_3	0.02	0.13	0.01	0.00	0.02	0.02	0.01	0.03	0.00	0.00
Fe_2O_3	2.15	2.87	1.36	1.75	1.58	0.88	1.86	2.31	1.16	1.13
FeO	27.83	23.8	24.75	24.25	25.45	28.75	25.51	25.14	26.11	25.85
MnO	0.79	0.92	0.84	0.86	0.89	0.72	0.82	0.91	0.81	0.83
MgO	3.61	6.32	6.51	6.85	5.62	3.67	6.13	5.62	5.37	5.44
CaO	7.20	6.93	6.66	6.88	6.97	7.20	6.30	7.09	7.18	7.00
Na_2O	0.00	0.05	0.02	0.00	0.07	0.01	0.02	0.01	0.00	0.00
K_2O	0.00	0.03	0.00	0.01	0.02	0.01	0.02	0.03	0.00	0.04
Total	98.88	100.33	99.49	100.05	100.03	100.10	99.29	100.47	100.14	99.81
(O)	12	12	12	12	12	12	12	12	12	12
Si	2.976	2.933	2.991	2.994	2.982	2.996	2.987	2.949	2.984	2.975
Ti	0.000	0.001	0.004	0.004	0.002	0.002	0.007	0.000	0.001	0.002

Al	1.917	1.966	1.934	1.905	1.952	1.952	1.907	1.969	1.961	1.983	
Cr^{3+}	0.001	0.008	0.001	0.000	0.001	0.001	0.001	0.002	0.000	0.000	
Fe^{3+}	0.130	0.168	0.080	0.102	0.093	0.052	0.110	0.135	0.068	0.066	
Fe^{2+}	1.870	1.545	1.617	1.574	1.662	1.902	1.679	1.637	1.706	1.692	
Mn	0.054	0.061	0.056	0.057	0.059	0.048	0.055	0.060	0.054	0.055	
Mg	0.432	0.731	0.758	0.792	0.654	0.433	0.719	0.652	0.625	0.635	
Ca	0.620	0.577	0.558	0.572	0.583	0.610	0.531	0.591	0.602	0.587	
Na	0.000	0.008	0.003	0.000	0.011	0.002	0.003	0.002	0.000	0.000	
K	0.000	0.003	0.000	0.001	0.002	0.001	0.002	0.003	0.000	0.004	
Sum	8.000	8.001	8.002	8.001	8.001	7.999	8.001	8.000	8.001	7.999	
X_{Grs}	0.14	0.12	0.15	0.14	0.15	0.18	0.13	0.13	0.17	0.17	
X_{Alm}	0.63	0.53	0.54	0.53	0.56	0.64	0.56	0.56	0.57	0.57	
X_{Py}	0.15	0.25	0.25	0.26	0.22	0.14	0.24	0.22	0.21	0.21	
X_{Sps}	0.02	0.02	0.02	0.02	0.02	0.02	0.02	0.02	0.02	0.02	
X_{Adr}	0.06	0.08	0.04	0.05	0.05	0.02	0.05	0.07	0.03	0.03	
Al^{T}	0.05	0.13	0.02	0.01	0.04	0.01	0.03	0.10	0.03	0.05	

Grt_2 = garnet of second generation, Grt_1 = garnet of earlier generation, Sil = sillimanite, bt = biotite, incl = inclusion, porb. = porphyroblast, cor = corona on, Opx = orthopyroxene, ilm = ilmenite, amp = amphibole, porc. = porphyroclast.

et al. (2008) demonstrated that an early granulite facies event was followed by intrusion of the Koraput Alkaline Complex; the entire ensemble then underwent a second granulite facies metamorphic event with P-T conditions and P-T trajectory similar to that documented for M_{2JP} in this study. Structural compatibility of the D_2 deformation in the Jeypore Province and the EGP, and the comparable metamorphic attributes indicate that the M_{2JP} and M_{2EG} events were time-equivalent and correspond to the same event.

Temporal constraints on the timing of the second granulite facies metamorphic overprint documented in this domain are difficult to ascertain from the existing age data. A preliminary report on the possible growth of metamorphic zircon in nepheline syenites within the Koraput Alkaline Complex (Hippe et al., 2008) has indicated a range (~880–700 Ma) of Neoproterozoic ages, which has been interpreted by them to represent repeated crystallization under high grade metamorphic condition. The older ages may also be interpreted as products of resetting of earlier magmatic ages, or as a series of events that affected the area in the mid-Neoproterozoic time. The interpretation is consistent with the intrusion age of 856 ± 18 Ma suggested from an earlier whole rock Rb–Sr study (Sarkar et al., 1989), and the U–Pb zircon ages of 917 Ma and 745 Ma inferred for the intrusion and metamorphism of the complex, respectively (Bhattacharya and Basei, 2010). An alternative interpretation is that all the above ages may reflect a degree of resetting by a later Pan-African thermal imprint that has been reported from this region (Mezger and Cosca, 1999). These dates, therefore, need to be corroborated by further detailed study, before they can be integrated into a temporally consistent tectonic model for the region. Nevertheless, there is little doubt that the observed tectonic imprint post-dates the pervasive late Mesoproterozoic Grenvillian ultrahigh temperature metamorphism in the EGP, and can therefore be consigned to the Neoproterozoic with some confidence, possibly around ~700 Ma, the latest time bracket on the obtained event.

The Jeypore Province, thus, underwent early granulite facies metamorphism in the Archean time. A second granulite facies event affected the eastern fringe of the province in the mid-Neoproterozoic; this latter event was shared with the western boundary of the Eastern Ghats Province. Also, as documented by Nanda et al. (2008) in the EGP, this second granulite event in the Jeypore Province also post-dates the D_2 and D_3 deformation events that was shared by both units across the contact.

9.2. Did the D_2 event juxtapose the Jeypore Province against the EGP?

West-vergent thrusting during D_2 deformation may possibly have been associated with the amalgamation of the Jeypore Province and the EGP. If the primary thrust plane along which movement occurred during D_2 is considered as the contact between the two provinces, then the EGP must represent the hangingwall block that was thrust over the footwall block represented by the Jeypore Province. This would explain parallelism of the S_2 shear fabric in both units across the contact, as the base of the hangingwall and top of the footwall would experience high shear strains. All earlier fabrics in both units would be rotated into parallelism with the new shear fabric, which is compatible with the structural observations in the contact zone.

The problem with this model is that the metamorphic evolution of the two units should theoretically vary subsequent to the thrusting event. While the footwall block (the Jeypore Province) would experience loading followed by heating due to thermal relaxation, the hangingwall block would be expected to undergo cooling and decompression (because of erosional unroofing). The results of this study, however, indicate that both units experienced a similar metamorphic history following the D_2 deformation event, involving heating followed by loading. While this may be explained by

Table 5
Composition of the major mineral phases present in quartzofeldspathic gneiss and feldspathic gneiss, and garnet–sillimanite gneiss of the EGP.

Rock type	Plagioclase		Clinopyroxenes		Orthopyroxene		Biotite		Garnet		
	$X_{An} \times 100$ Matrix	Inclusions in Grt or Kfs rims	$X_{Mg} \times 100$	Al_2O_3 wt%	$X_{Mg} \times 100$	Al_2O_3 wt%	$X_{Mg} \times 100$	TiO_2 wt%	X_{Alm}	X_{Py}	X_{Gr}
Quartzofeldspathic/ feldspathic gneiss*	21–44	44–48	63–75	0.49–1.75	44–58	–	44–51	5.07–7.03	0.59–0.65	0.13–0.20	0.11–0.20
Garnet–sillimanite gneiss							55–64		0.61–0.64	0.31–0.34	<0.05

* Data reproduced for quartzofeldspathic/feldspathic gneiss, summarized from Nanda et al. (2008).

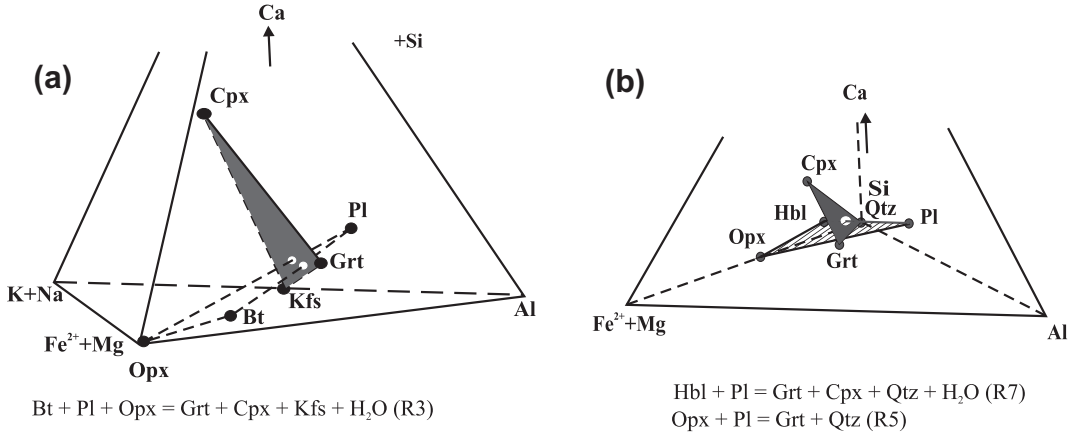

Fig. 5. (a) Al–(Fe^{+2} + Mg)–(K + Na)–Ca chemographic projection diagram showing participating phases and reactions inferred in charno-enderbite of the Jeypore Province. (b) Al–(Fe^{+2} + Mg)–Si–Ca chemographic projection diagram showing possible metamorphic reactions in rocks of Jeypore Province. Note that orthopyroxene (Opx), garnet (Grt), plagioclase (Pl) and quartz (Qtz) are co-planar.

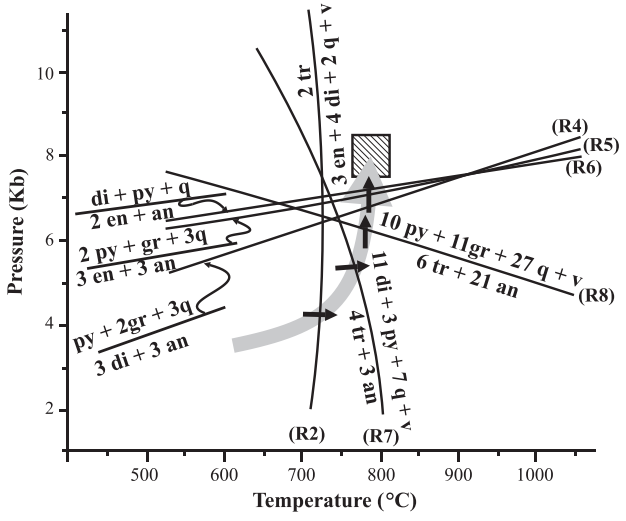

Fig. 6. Reactions inferred from textural relations (curves R1–R8) plotted in P-T space at a (H_2O) = 0.1 using THERMOCALC v. 3.21. The reactions are labelled in accordance with the corresponding reactions mentioned in the text and the abbreviations used are the same as those in THERMOCALC. The reactions are plotted to indicate the sense in which they were crossed (indicated in short dark arrows) during the P-T evolution. The larger curved arrow indicates a possible P-T trajectory that is compatible with both the sense and the sequence of crossing of individual reactions (see text) during the second granulite facies metamorphic event.

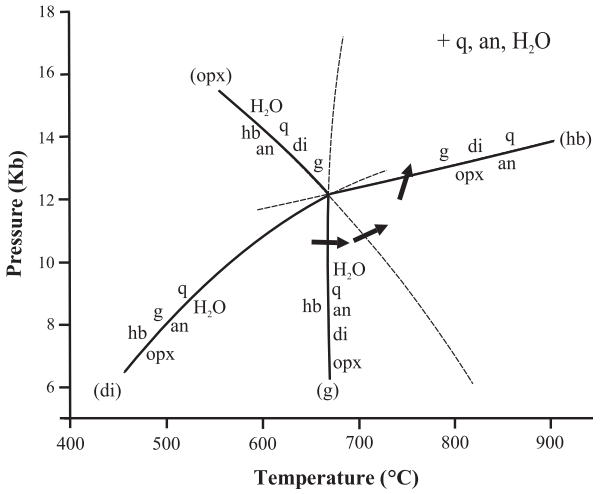

Fig. 7. Schreinemakers construction around an invariant point in the CMASH system, involving the seven phases hornblende, orthopyroxene, diopside (clinopyroxene), garnet, anorthite (plagioclase), quartz and water (in fluid). Anorthite, quartz and fluid (with $a_{H_2O} = 0.1$) are considered to be in excess, as appropriate to the enderbites. The construction demonstrates the sequence in which the documented textural reactions in the enderbites were crossed during the second granulite facies metamorphic event (M_{2JP}). As shown, hornblende breaks down on its own composition by reaction (g); if any hornblende survives metastably, it would be eliminated from the matrix assemblage by the metastable extension of reaction (opx). Finally, the assemblage garnet + clinopyroxene + quartz is introduced into the assemblage by reaction (hb). The sequence suggests a heating followed by cooling trajectory.

Table 6
Results of thermobarometric calculations from charnockitic suite of rocks in the JP.

Sample	Textural locale	T°C$_{EG}$	T°C$_{Gly}$	T°C$_{Kr}$	T°C$_{Pow}$	T°C$_{GP}$	T°C $_{Hr}$	T°C$_{FS}$	T°C$_{Dg}$	P$_{Ref}$ kb
K279 Grt70 Cpx72	Grt$_2$ (corona)–Cpx$_1$ (inclusion in Grt)	697	727	635	675					8
K279 Grt71 Cpx75	Grt$_2$ (corona)–Cpx$_1$ (inclusion in Grt)	673	709	608	651					8
K280a Grt29 Cpx25	Grt$_2$ (corona)–Cpx$_1$ (core)	715	731	664	695					8
K280a Grt29 Cpx24	Grt$_2$ (corona)–Cpx$_1$ (core)	778	784	733	759					8
K280a Grt30 Cpx28	Grt$_2$ (corona)–Cpx$_1$ (rim)	661	688	603	640					8
K280a Grt67 Cpx69	Grt$_2$(rim)–Cpx$_2$ (rim)	725	742	673	705					8
K279 Grt98 Hbl96	Grt$_2$ (porb. core)–Hbl (inclusion in Grt)					614				
K279 Grt84 Hbl81	Grt$_2$ (porb. core)–Hbl (inclusion in Grt)					645				
K279 Grt82 Hbl81	Grt$_2$ (porb. rim)–Hbl (inclusion in Grt)					617				
K280a Grt119 Hbl108	Grt$_2$ (rim)–Hbl (mosaic)					730				
K280a Grt119 Hbl111	Grt$_2$ (rim)–Hbl (mosaic)					722				
K280a Grt40 Opx39	Grt$_2$ (corona)–Opx$_2$ (rim)		661				607			8
K280a Grt67 Opx66	Grt$_2$ (corona)–Opx$_2$ (rim)		704				650			8
K280a Grt68 Opx64	Grt$_2$ (corona)–Opx$_2$ (core)		786				733			8
K286a Grt4 Opx15	Grt$_2$ (core)–Opx$_2$ (core)		778							
K286a Grt6 Bt2	Grt$_2$ (rim)–Bt (inclusion)							748	725	8
K286a Grt4 Bt1	Grt$_2$ (core)–Bt (inclusion)							770	745	8
K286a Grt35 Bt30	Grt$_2$ (core)–Bt (inclusion)							807	776	8

		P$_{NP}$	P Moecher				P$_{KS}$	T°C Ref
			GAHS	GADS	GAFS		P$_{Mg}$/P$_{Fe}$	
K280a Grt29 Cpx24 Pl32	Grt$_2$ (corona)–Cpx$_1$ (core)–Pl (matrix)	8.5	8.2	7.0				750
K280a Grt29 Cpx25 Pl32	Grt$_2$ (corona)–Cpx$_1$ (core)–Pl (matrix)		8.0	6.0				750
K280a Grt68 Opx64 Cpx71 Pl72	Grt$_2$ (corona)–Opx$_2$ (core)–Cpx$_2$ (rim)–Pl (matrix)		7.5	6.6	8.1			750
K280a Grt67 Opx66 Cpx71 Pl72	Grt$_2$ (corona)–Opx$_2$ (rim)–Cpx$_2$ (rim)–Pl (matrix)		7.5	6.0	8.5			750
K280a Grt40 Opx39 Cpx45 Pl51	Grt$_2$ (corona)–Opx$_2$ (rim)–Cpx$_2$ (rim)–Pl (matrix)		8.5	5.8	8.6			750
K279 Grt98 Hbl96 Pl87	Grt$_2$ (porb. core)–Hbl (inclusion)–Pl (matrix)						7.7/8.6	750
K279 Grt84 Hbl81 Pl87	Grt$_2$ (porb. core)–Hbl (inclusion)–Pl (matrix)						7.4/8.1	750

Grt: garnet, Cpx: clinopyroxene, Pl: plagioclase, Hbl: Hornblende, Opx: orthopyroxene, Bt: biotite, EG: Ellis and Green, 1979; Kr: Krogh, 1988; Pow: Powell, 1985; GP: Graham and Powell, 1984; Hr: Harley, 1984; FS: Ferry and Spear, 1978; Dg: Dasgupta et al., 1991; Gly: Ganguly et al., 1996; NP: Newton and Perkins, 1982; KS: Kohn and Spear, 1990; GAHS: Grt–Pl–Hed–Qtz, GADS: Grt–Pl–Di–Qtz, GAFS: Grt–Pl–Fs–Qtz, Ref: reference, porb.: porphyroblast

Table 7
Average PT calculation using THERMOCALC v. 3.21.

Independent set of reactions used for average P-T calculation	Mineral assemblage used
(1) en + gr + q = 2di + an (2) gr + 2py + 3q = 3en + 3an (3) alm + 3hed = 3 fs + gr (4) 2alm + gr + 3q = 3 fs + 3an	From Hbl and Bt absent micro-domain in charnockites of the JP: K 280a = Pl 72, Cpx 69, Opx 64, Grt 67, Qtz
Av P = 7.6 ± 1.5 kb, Av *T* = 765 ± 120 °C, significant fit for 95% confidence = 0.13	
Independent set of reactions used for average P-T calculation	Mineral assemblages used
(1) gr + 2py + 3q = 3an + 3en (2) 2gr + py + 3q = 3an + 3di (3) gr + 2alm + 3q = 3an + 3 fs (4) 2gr + alm + 3q = 3an + 3hed (5) 21an + 6ftr = 11gr + 10alm + 27q + 6H$_2$O (6) 8py + 6tr = 2gr + 6an + 27en + 6H$_2$O (7) 12an + 18en + 3parg = 4gr + 11py + 3ab + 3tr	From Hbl bearing micro-domain in charnockites of the JP: K 279 = Grt 98, Hbl 96, Pl 87, Cpx 95, Opx 52, Qtz
Av P = 8.7 ± 1.0 kb, Av *T* = 766 ± 35 °C, significant fit for 95% confidence = 0.85, $a_{H_2O} = 0.2$	

NB: Abbreviation of end members in accordance with THERMOCALC v. 3.21

crustal thickening synchronized with fast convective thinning of the lithospheric mantle, as suggested by Nanda et al. (2008), the model applies equally to both blocks. In other words, prior to the M_2 metamorphic cycle, the Jeypore Province and EGP must already have been amalgamated into a single block that was in similar thermal condition. Since both blocks experienced loading during west-vergent D_2 thrusting, the thrust plane itself must be located further to the east, well within the EGP. Thus, while some relative movement between the Jeypore and Eastern Ghats Provinces may have occurred during D_2 deformation, this event cannot be considered to have effected amalgamation of the two units, since they were already welded together.

9.3. Implications for the nature of the Jeypore Province–EGP contact

The implication of the above is that at least in the Neoproterozoic, prior to the D_2 deformation, the EGP and the Jeypore Province were already amalgamated into a single craton. This may contradict the suggestion of Simmat and Raith (2008) that the Jeypore Province became an integral part of the Indian craton during a late Archean tectono-thermal event, that implies that the Jeypore Province–EGP contact represents the site of the India–Antarctica collision either during the Grenvillian or the Pan-African time (Aftalion et al., 2000; Upadhyay, 2008; Mukhopadhyay and Basak, 2009). It has been argued (Dobmeier and Raith, 2003; Simmat and

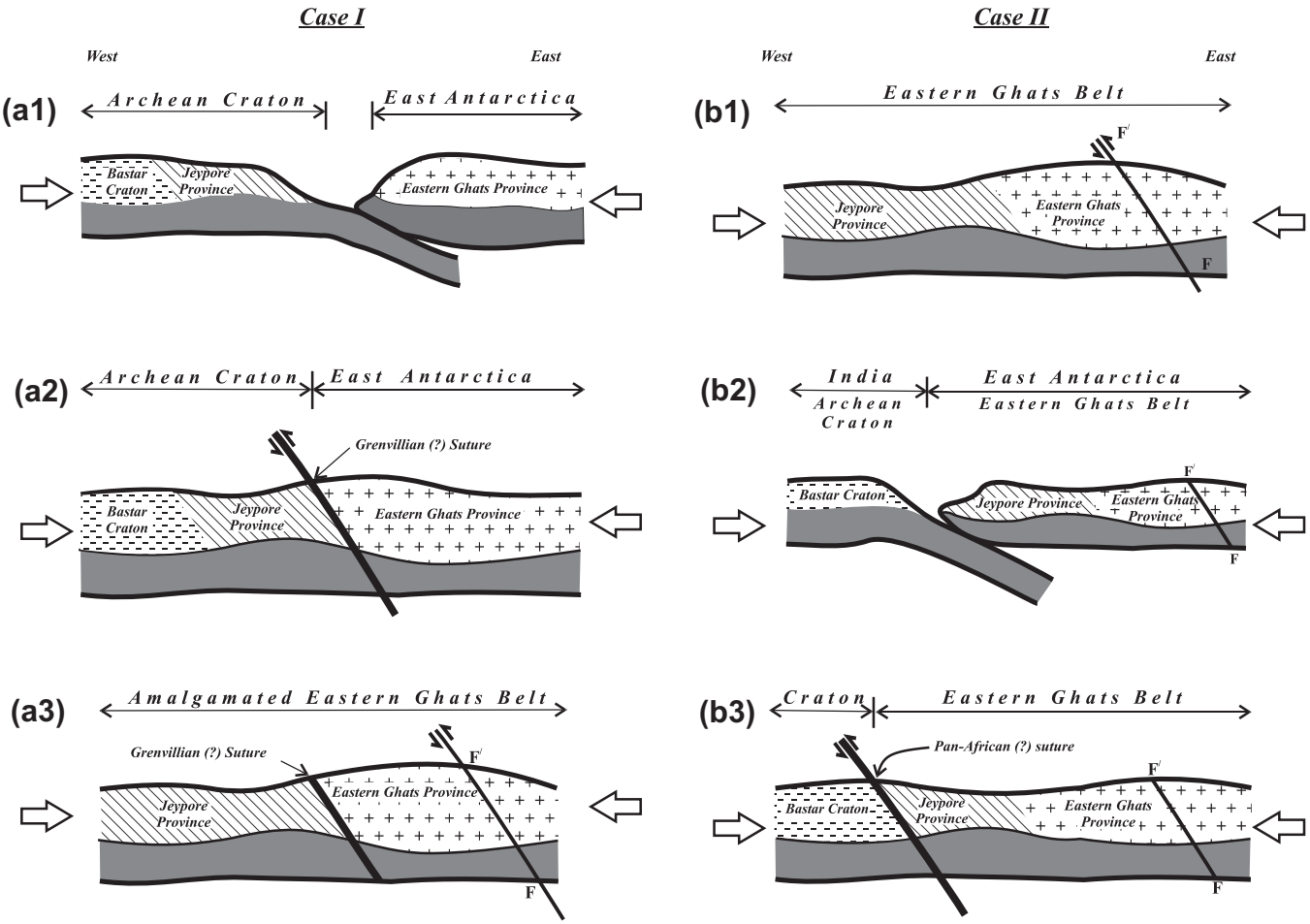

Fig. 8. Schematic sections to illustrate the possible sequence of tectonic events that affected the study area. *Case I*. The Jeypore Province is considered to be a component of the Archean craton (a1) that collided with the Eastern Ghats Province in the Grenvillian time (a2). Subsequently, intracontinental shortening occurred on thrust FF rooted to the east (a3), in the interior of the Eastern Ghats Province. *Case II*. The Jeypore Province is considered to be amalgamated with the Eastern Ghats Province within the Eastern Ghats Belt (b1). The amalgamated unit initially experiences intracontinental shortening along thrust FF (b1), and then over-rides the Indian cratoni plate in the west (b2). Collision occurs subsequently (b3) in the Pan-African time, but the suture is located along the contact between the Jeypore Province and the Bastar craton, and not along the EGP–Jeypore Province contact.

Raith, 2008) based on existing isotope data from the Jeypore Province (Rickers et al., 2001; Kovach et al., 2001) that the last thermotectonic event in the Jeypore Province is Archean in age. The present study also suggests that at least along the eastern fringe of the Jeypore Province, there is evidence for a much later (probably Neoproterozoic) tectonic event. This later event also affected the western part of the EGP.

Nanda et al. (2008) argued that the absence of any obducted oceanic crust, arc-related magmatism or post-collisional granitoid intrusion of Neoproterozoic age in the Koraput area was not compatible with a model of subduction involving consumption of an ocean basin that culminated in continent–continent collision. While obducted oceanic crust may well have been removed by erosion, it is difficult to explain the absence of arc-magmatism or later granitoid intrusion in a collisional setting. The continuity in structural fabric across the contact between the two units, and more importantly, the similarity of their post-D_2 metamorphic evolution indicate that the two units were part of the same footwall block during D_2 thrusting. The amalgamated units were overthrust by a block that was transported from east to west during west-vergent thrusting. The entire sequence of D_2 deformation can therefore only be interpreted to be intracontinental in nature. The Jeypore and Eastern Ghats Provinces, in other words, were already part of the same continental block by the mid-Neoproterozoic.

9.4. The EGB–craton contact: recognizing the suture

A suture zone is defined as a boundary between crustal blocks that originally belonged to two different tectonic plates, and were subsequently juxtaposed by plate motion (Moores and Twiss, 1995). The EGB-craton contact is generally considered to be a suture based on the following evidence: (1) presence of tectonic mélanges and ophiolitic fragments (Dharma Rao and Reddy, 2009; Dharma Rao et al., 2011), that testify to the presence of an intervening ocean; (2) presence of a linear belt of deformed alkaline complexes (DARs) along the EGB-craton contact (Ramakrishnan et al., 1998; Chetty and Murthy, 1998; Gupta and Bose, 2004; Gupta et al., 2005; Upadhyay, 2008; see Fig. 1b), supposedly representative of a suture (after Burke et al., 2003); and (3) evidence for hot-over-cold thrusting along the contact, with hot EGB granulites from deep crustal levels syn-metamorphically emplaced onto the cold craton (Gupta et al., 2000; Bhadra et al., 2004), leading to the development of an inverted metamorphic gradient in the footwall of the suture (e.g. Duebendorfer, 1988).

Presence of ophiolitic fragments constitute the most definitive evidence of a suture zone. Unfortunately, in the context of the EGB, such evidence (e.g. Dharma Rao et al., 2011) is restricted to the contact with the Dharwar craton, south of the Godavari rift. North of the rift, the EGB–Bastar craton contact is not characterized

by any mélanges or ophiolitic components. However, the linear zone of deformed alkaline complexes that extends from Elchuru and Kunavaram along the EGB-Dharwar contact south of the Godavari rift, into the Khariar and Rairakhol complexes along the contact with the Bastar craton, may represent the fossilized suture zone. All these complexes lie precisely on the contact between the granulite belt in the east and lower grade metamorphic rocks of the craton to the west. Unlike the other alkaline plutons, the Koraput complex lies to the east of the "charnockite line" of Fermor (1936) that otherwise coincides perfectly with the DAR line. Available geochronological data for the Koraput complex (Sarkar et al., 1989; Hippe et al., 2008; Bhattacharya and Basei, 2010) also differ from the Mesoproterozoic intrusion ages (see Upadhyay, 2008 for summary) inferred for the other plutons. The EGP–Jeypore Province contact, that passes 3 km west of the Koraput complex and separates two essentially granulite provinces (Fig. 2), can therefore not be considered coincident with any suture defined by the DAR line.

In this context, it is also important to compare the structural and metamorphic evolution across the Eastern Ghats Province–Bastar Craton boundary further to the north in the Deobhog area (Gupta et al., 2000; Bhadra et al., 2004). Following juxtaposition, the Eastern Ghats unit in the hanging wall underwent cooling and decompression, while the cratonic foreland was characterized by heating; Gupta et al. (2000) interpreted this to be a consequence of hot-over-cold thrusting, with sequential fabric formation in the footwall as the isotherms progressively migrated into the foreland of the thrust (Bhadra et al., 2004). These observations contrast sharply with the present study, where the post-juxtaposition P-T paths across the litho-tectonic contact between the EGP and the Jeypore Province are closely comparable. Indeed, the post-D_2 thermal evolution cannot be explained by a model of 'hot-over-cold' thrusting. This reiterates the contention of this study, that the tectonics of the present study area is not compatible with a model of a hot mobile belt in the hangingwall being thrust over a cold cratonic footwall. It is much more likely in that both units in the present study (i.e. the EGP and the Jeypore Province) lie in the footwall of a major thrust zone that lies eastward within the EGP.

9.5. Tectonic implications

The implication of the above study is that if continent–continent collision did occur along the Jeypore Province–EGP boundary, it must be older than the M_{2JP} granulite event documented in this study. Significant granitoid magmatism in the EGP is last recorded from 980 to 930 Ma, during the emplacement of the megacrystic granitoids (Mezger and Cosca, 1999). No comparable ages for granulite facies metamorphism have yet been obtained from the Jeypore Province, which is unusual if it was the frontal zone of a subducting continental plate that was involved in collision. Nevertheless, this remains the only possibility if the contact between the two provinces is indeed a suture. Alternatively, the EGP unit in the present study must simply be regarded as a para-autochthonous unit that was juxtaposed against the rigid Archean buttress of the Jeypore Province in the mid-Neoproterozoic. Either way, the existence of a phase of intracontinental shortening and resultant granulite metamorphism in the Eastern Ghats Belt appears inescapable.

From the perspective of assembly of the Indian shield, this suggests two possible scenarios: *Case I*. The Archean cratonic nucleus that included the Jeypore Province in its frontal part, collided with the frontal part of the East Antarctica plate (i.e. the Eastern Ghats Province) in the Grenvillian time (Fig. 8, a1 and a2), and subsequently the amalgamated granulite unit (i.e., the Eastern Ghats Belt, including both the EGP and the Jeypore Province) underwent intracontinental shortening along thrust FF located east of the Grenvillian suture, within the EGP (Fig. 8, a3); or *Case II*. The amalgamated EGP–Jeypore Province unit, representing the Eastern Ghats Belt, was essentially a part of the East Antarctica plate that experienced intracontinental shortening along thrust FF in the mid-Neoproterozoic (Fig. 8, b1), and only subsequently collided with the Archean Indian craton, possibly in the Pan-African time (Fig. 8, b2 and b3). In the first case, the EGP–Jeypore Province contact represents a older suture that has subsequently been reworked during the intracontinental orogeny associated with fault FF; in the second case, this contact does not represent the site of a collision, and a suture, if at all present, must be located along the *western*, and not the eastern boundary of the Jeypore Province. The Jeypore Province may well represent the western flank of the basin in which the sediments of the EGP were initially deposited, as suggested by Gupta (in press). On the basis of the present study, the second possibility appears more credible.

Acknowledgements

The authors are indebted to Dr. C.V. Dharma Rao and an anonymous reviewer for critical reviews of the earlier draft of the manuscript, that has helped improve the final version substantially. Prof. M. Santosh is thanked for the excellent editorial processing of the manuscript. The authors also very gratefully acknowledge the enormous help and encouragement obtained from Profs. H.C. Dasgupta and C. Bhattacharya. Thanks are due to Mr. Tutu Panda and other members of "Atithi Bhaban" guest house (Koraput, India) for their hospitality during fieldwork. Dr. Sudipta Sarkar is thanked profusely for help during manuscript preparation.

Appendix A. Supplementary material

Supplementary data associated with this article can be found, in the online version, at doi:10.1016/j.jseaes.2011.10.001.

References

Aftalion, M., Bowes, D.R., Dash, B., Dempster, T.J., 1988. Late Proterozoic charnockites of Orissa, India—a U–Pb and Rb–Sr isotopic study. Journal of Geology 96, 663–676.

Aftalion, M., Bowes, D.R., Dash, B., Fallick, A.E., 2000. Late Pan-African thermal history in the Eastern Ghats Terrane, India, from U–Pb and K–Ar isotopic study of the Mid-Proterozoic Khariar alkali syenite, Orissa. Geological Survey of India, Special Publication 57, 26–33.

Bhadra, S., Gupta, S., Banerjee, M., 2004. Structural evolution across the Eastern Ghats Mobile Belt – Bastar craton boundary, India: hot over cold thrusting in an ancient collision zone. Journal of Structural Geology 26, 233–245.

Bhattacharya, S., Basei, M., 2010. Contrasting magmatic signatures in the Rairakhol and Koraput alkaline complexes, Eastern Ghats Belt, India. Journal of Earth System Science, Indian Academy of Science 119, 175–181.

Boger, S.D., 2011. Antarctica – before and after Gondwana. Gondwana Research 19, 335–371.

Boger, S.D., Carson, C.J., Wilson, C.J.L., Fanning, C.M., 2001. Early Palaeozoic tectonism within East Antarctic Craton; the final suture between East and West Gondwana? Geology 29, 463–466.

Boger, S.D., Carson, C.J., Wilson, C.J.L., Fanning, C.M., 2000. Neoproterozoic deformation in the Radlok Lake region of the northern Prince Charles Mountains East Antarctica; evidence for a single protracted orogenic event. Precambrian Research 104, 1–24.

Burke, K., Ashwal, L.D., Webb, S.J., 2003. New way to map old sutures using deformed alkaline rocks and carbonatites. Geology 31, 391–394.

Chetty, T.R.K., 2010. Structural architecture of the northern composite terrane, the Eastern Ghats Belt, India: implications for Gondwana tectonics. Gondwana Research 18, 565–582.

Chetty, T.R.K., Murthy, D.S.N., 1993. Landsat thematic mapper data applied to structural studies of the Eastern Ghats Granulite Terrane in parts of Andhra Pradesh. Journal of Geological Society of India 42, 373–391.

Chetty, T.R.K., Murthy, D.S.N., 1994. Collision tectonics in the Eastern Ghats Mobile Belt: mesoscopic to satellite scale structural observations. Terra Nova 6, 72–81.

Chetty, T.R.K., Murthy, D.S.N., 1998. Elchuru – Kunavaram – Koraput (EKK) Shear zone, Eastern Ghats granulite terrane, India: a possible Precambrian suture zone. In: Rao, A.T., Divi, S.R., Yoshida, M. (Eds.), Precambrian crustal processes in East Gondwana. Gondwana Research Group Memoir 4, pp. 37–48.

Collins, A.S., Pisarevsky, S.A., 2005. Amalgamating Eastern Gondwana: the evolution of the Circum-Indian Orogens. Earth-Science Review 7, 229–270.
Crookshank, H., 1938. The western margin of the Eastern Ghats in southern Jeypore. Records, Geological Survey of India 73, 398–434.
Dalziel, I.W.D., 1991. Pacific margins of Laurentia and East Antarctica–Australia as a conjugate rift pair: evidence and implications for an Eocambrian supercontinent. Geology 19, 598–601.
Dasgupta, S., Sengupta, P., 2003. Indo-Antarctica correlation: a perspective from the Eastern Ghats Belt. In: Yoshida, M., Windley, B.F., Dasgupta, S. (Eds.), Proterozoic East Gondwana: Supercontinent Assembly and Breakup. Geological Society of London, Special Publication 206, pp. 131–143.
Dasgupta, S., Sengupta, P., Guha, D., Fukuoka, M., 1991. A refined garnet–biotite Fe–Mg exchange geothermometer and its application in amphibolites and garnulites. Contributions to Mineralogy and Petrology 109, 130–137.
Dasgupta, S., Sengupta, P., Fukuoka, M., Chakraborty, S., 1992. Dehydration melting, fluid buffering and decompression P-T path in a granulite complex from the Eastern Ghats, India. Journal of Metamorphic Geology 10, 777–788.
Dasgupta, S., Sengupta, P., Ehl, J., Raith, M., Bardhan, S., 1995. Reaction textures in a suite of spinel granulites from the Eastern Ghats Belt, India: evidence for polymetamorphism, a partial petrogenetic grid in the system KFMASH and the roles of ZnO and Fe_2O_3. Journal of Petrology 36, 435–461.
Dharma Rao, C.V., Reddy, U.V.B., 2009. Petrological and geochemical characterization of Ophiolite mélange, Nellore–Khammam schist belt, SE India. Journal of Asian Earth Sciences 65, 261–276.
Dharma Rao, C.V., Santosh, M., Wu, Y.-B., 2011. Mesoproterozoic ophiolitic mélange from the SE periphery of the Indian plate: U–Pb zircon ages and tectonic implications. Gondwana Research 19, 384–401.
Dobmeier, C., and Raith, M., 2003. Crustal architecture and evolution of the Eastern Ghats Belt and adjacent regions of India. In: Yoshida, M., Windley, B.F., Dasgupta, S. (Eds.), Proterozoic East Gondwana: Supercontinent Assembly and Breakup. Geological Society of London, Special Publication 206, pp. 145–168.
Dodson, M.H., 1973. Closure temperature in cooling geochronological and petrological systems. Contributions to Mineralogy and Petrology 40, 259–274.
Duebendorfer, E.M., 1988. Evidence for an inverted metamorphic gradient associated with a Precambrian suture, southern Wyoming. Journal of Metamorphic Geology 6, 41–63.
Ellis, D.J., Green, E.H., 1979. An experimental study of the effect of Ca upon garnet–clinopyroxene Fe–Mg exchange equilibria. Contributions to Mineralogy and Petrology 71, 13–22.
Fermor, L.L., 1936. An attempt at the correlation of the ancient schistose formations of peninsular India. Memoir, Geological Survey of India 70, 217.
Ferry, J.M., Spear, F.S., 1978. Experimental calibration of the partitioning of Fe and Mg between biotite and garnet. Contributions to Mineralogy and Petrology 78, 113–117.
Fitzsimons, I.C.W., 2000. A review of tectonic events in the East Antarctic Shield and their implications for Gondwana and earlier supercontinents. Journal African Earth Science 31, 2–23.
Fitzsimons, I.C.W., Harley, S.L., 1995. Garnet coronas in scapolite–wollastonite calc-silicates from East Antarctica: the application and limitations of activity-corrected grids. Journal of Metamorphic Geology 12, 761–777.
Ganguly, J., Cheng, W., Tirone, M., 1996. Thermodynamics of aluminosilicate garnet solid solutions: new experimental data, an optimized model and thermometric applications. Contributions Mineralogy and Petrology 126, 137–151.
Graham, C.M., Powell, R., 1984. A garnet–hornblende geothermometer: calibration, testing, and application to the Pelona Schist, Southern California. Journal of Metamorphic Geology 2, 13–21.
Grew, E.S., Manton, W.I., 1986. A new correlation of sapphirine granulites in the Indo-Antarctic metamorphic terrane: late Proterozoic dates from the Eastern Ghats. Precambrian Research 33, 123–139.
Gupta, S., 2004. The Eastern Ghats Belt, India – a new look at an old orogen. In: Uniformitarianism revisited – comparison between ancient and modern orogens of India. Geological Survey of India. Special Publication 84, pp. 75–100.
Gupta, S., in press. Strain localization, granulite formation and geodynamic setting of 'hot orogens': a case study from the Eastern Ghats Province, India. Geological Journal. doi:10.1002/gj.1328.
Gupta, S., Bose, S., 2004. Deformation history of the Kunavaram Complex, Eastern Ghats Belt, India: implications for alkaline magmatism along the Indo-Antarctica suture. Gondwana Research (Gondwana Newsletter Section) 7, 1228–1335.
Gupta, S., Bhattacharya, A., Raith, M., Nanda, J.K., 2000. Pressure–temperature – deformational history across a vestigial craton–mobile belt boundary: the western margin of the Eastern Ghats Belt at Deobhog, India. Journal of Metamorphic Geology 18, 683–697.
Gupta, S., Nanda, J., Mukherjee, S., Santra, M., 2005. Alkaline magmatism versus collision tectonics in the Eastern Ghats belt, India: contraints from structural studies in the Koraput complex. Gondwana Research 8, 403–419.
Harley, S.L., 1984. An experimental study of the partitioning of Fe and Mg between garnet and orthopyroxene. Contributions to Mineralogy and Petrology 86, 359–373.
Harley, S.L., 2003. Archean–Cambrian crustal development of East Antarctica: metamorphic characteristics and tectonic implications. In: Yoshida, M., Windley, B.F., Dasgupta, S. (Eds.) Proterozoic East Gondwana: Supercontinent Assembly and Breakup. Geological Society London, Special Publication 206, pp. 203–230.
Hippe, K., Hammerschmidt, K., Dobmeier, C.J., 2008. Evidence of Metamorphic Zircon Growth in Zr-Depleted Nepheline Syenite. Europ. Geoscience Union Gen. Ass, Vienna, Austria, 13–18 April 2008, Abstract Volume.
Hoffman, P.F., 1989. Speculations on Laurentia's first gigayear (2.0–1.0 Ga). Geology 17, 135–138.
Hoffman, P.F., 1991. Did the breakout of Laurentia Turn Gondwanaland inside-out? Science 252 (5011), 1409–1412.
Kelly, N.M., Clarke, G.L., Fanning, C.M., 2002. A two-stage evolution of the Neoproterozoic Rayner Structural Episode: new U–Pb sensitive high resolution ion microprobe constraints from the Oygarden Group, Kemp Land, East Antarctica. Precambrian Research 116, 307–330.
Kohn, M.J., Spear, F.S., 1990. Two new geobarometers for garnet amphibolites, with applications to southeast Vermont. American Mineralogist 75, 89–96.
Korhonen, F.J., Saw, A.K., Clark, C., Brown, M., Bhattacharya, S., 2011. New constraints on UHT metamorphism in the Eastern Ghats Province through the application of phase equilibria modeling and *in situ* geochronology. Gondwana Research. doi:10.1016/j.gr.2011.05.006.
Kovach, V.P., Simmat, R., Rickers, K., Berezhnaya, E.B., Salnikova, E.V., Dobmeier, C., Raith, M., Yakovleva, S.Z., Kotov, A.B., 2001. The Western Charnockite Zone of the Eastern Ghats Belt, India – an independent crustal province of Late Archean (2.8 Ga) and Palaeoproterozoic (1.7–1.6 Ga) terrains. Gondwana Research 4, 666–667.
Kretz, R., 1983. Symbols for rock forming minerals. American Mineralogist 68, 277–279.
Krogh, E.J., 1988. The garnet–clinopyroxene Fe–Mg geothermometer – a reinterpretation of existing experimental data. Contributions to Mineralogy and Petrology 99, 4–48.
Kruhl, J.H., 1996. Prism- and basal-plane parallel subgrain boundaries in quartz: a microstructural geothermobarometer. Journal of Metamorphic Geology 14, 581–589.
Li, Z.X., Bogdanova, S.V., Collins, A.S., Davidson, A., Waele, B.De., Ernst, R.E., Fitzsimons, I.C.W., Fuck, R.A., Gladkochub, D.P., Jacobs, J., Karlstrom, K.E., Lu, S., Natapov, L.M., Peas, V., Piserevsky, S.A., Thrane, K., Vernikovsky, V., 2008. Assembly, configuration, and break-up history of Rodinia: a synthesis. Precambrian Research 168, 179–210.
Meert, J.G., 2002. Paleomagnetic evidence for a Paleo-Mesoproterozoic supercontinent Columbia. Gondwana Research 5, 207–216.
Meert, J.G., Pandit, M.K., Pradhan, V.M., Kaemnov, G., 2011. Preliminary report on the paleomagnetism of 1.88 Ga dykes from the Bastar and Dharwar cratons, Peninsular India. Gondwana Research 20, 335–343.
Mezger, K., Cosca, M.A., 1999. The thermal history of the Eastern Ghats Belt (India), as revealed by U–Pb and ^{40}Ar–^{39}Ar dating of metamorphic and magmatic minerals: implications for the SWEAT correlation. Precambrian Research 94, 251–271.
Moecher, D.P., Essene, E.J., Anovitz, L.M., 1988. Calculation and application of clinopyroxene–garnet–plagioclase–quartz geobarometers. Contributions to Mineralogy and Petrology 100, 92–106.
Moores, E.M., 1991. Southwest US-East Antarctic (SWEAT) connection: a hypothesis. Geology 19, 425–428.
Moores, E.M., Twiss, R.J., 1995. Tectonics. W.H. Freeman and Company.
Mukhopadhyay, D., Basak, K., 2009. The Eastern Ghats Belt – a polycyclic terrain. Journal of Geological Society of India 73, 489–518.
Nanda, J., Gupta, S., 2008. Late tectonic imprints on the Archean Jeypore Province – implications for assembly of the Indian shield. In: International Conference on Geology – Indian Scenario and Global Context, Indian Statistical Institute, Kolkata (January 7–11), Program and Abstracts, p. 65A.
Nanda, J., Gupta, S., Dobmeier, C.J., 2008. Metamorphism of the Koraput Alkaline complex, Eastern Ghats Province, India – evidence for reworking of a granulite terrane. Precambrian Research 165, 153–168.
Nanda, J., Gupta, S., Mamtani, M.A., 2009. Analysis of deformation fabric in an alkaline complex (Koraput, India): implications for time relationship between emplacement, fabric development and regional tectonics. Journal of Geological Society of India 74, 78–94.
Nanda, J.K., Pati, U.C., 1989. Field relations and petrochemistry of the granulites and associated rocks in the Ganjam–Koraput sector of the Eastern Ghats Belt. Indian Mineral 43, 247–264.
Narayanaswami, S., 1975. Proposal for charnockite–khondalite system in the Archean Shield of Peninsular India. Geological Survey of India. Miscellaneous Publication 23, 1–16.
Newton, R.C., Perkins, D., 1982. Thermodynamic calibration of geobarometers based on the assemblages garnet–plagioclase–orthopyroxene (clinopyroxene)–quartz. American Mineralogist 67, 203–222.
Paul, D.K., Ray Barman, T.K., McNaughton, N.J., Fletcher, I.R., Potts, P.J., Ramakrishnan, M., Augustine, P.F., 1990. Archean–Proterozoic evolution of Indian charnockites: isotopic and geochemical evidence from granulites of the Eastern Ghats Belt. Journal of Geology 98, 253–263.
Powell, R., 1985. Regression diagonistics and robust regression in geothermometer/geobarometer calibration: the garnet–clinpyroxene geothermometer revisited. Journal of Metamorphic Geology 3, 231–243.
Ramakrishnan, M., Nanda, J.K., Augustine, P.F., 1998. Geological evolution of the Proterozoic Eastern Ghats Mobile Belt. Geological Survey of India, Special Publication 44, 1–21.
Rickers, K., Mezger, K., Raith, M.M., 2001. Evolution of the continental crust in the Proterozoic Eastern Ghats Belt, India and new constraints for Rodinia reconstruction: implications from Sm–Nd, Rb–Sr and Pb–Pb isotopes. Precambrian Research 112, 183–210.
Rogers, J.J.W., Santosh, M., 2002. Configuration of Columbia, a Mesoproterozoic Supercontinent. Gondwana Research 5, 5–22.
Rogers, J.J.W., Santosh, M., 2009. Tectonics and surface effects of the supercontinent Columbia. Gondwana Research 15 (3–4), 373–380.

Santosh, M., 2010. A synopsis of recent conceptual models on supercontinent tectonics in relation to mantle dynamics, life evolution and surface environment. Journal of Geodynamics 50, 116–133.

Santosh, M., Maruyama, S., Yamamoto, S., 2009. The making and breaking of supercontinents: some speculations based on superplume, superdownwelling and the role of tectosphere. Gondwana Research 15, 324–341.

Sarkar, G., Corfu, F., Paul, D.K., McNaughton, N.J., Gupta, S.N., Bishui, P.K., 1993. Early Archean crust in Bastar craton, Central India—a geochemical and isotopic study. Precambrian Research 62, 127–137.

Sarkar, A., Nanda, J.K., Paul, D.K., Bishui, P.K., Gupta, S.N., 1989. Late Proterozoic alkaline magmatism in the Eastern Ghats Belt: Rb–Sr isotopic study on the Koraput Complex, Orissa. Indian Minerals 43, 265–272.

Sengupta, P., Dasgupta, S., Bhattacharya, P.K., Fukuoka, M., Chakraborti, S., Bhowmik, S., 1990. Petro-tectonic imprints in the sapphirine granulites from Anantagiri, Eastern Ghats Mobile Belt, India. Journal of Petrology 31, 971–996.

Shaw, R.K., Arima, M., Kagami, H., Fanning, C.M., Shiraishi, K., Motoyoshi, Y., 1997. Proterozoic events in the Eastern Ghats Granulite Belt, India: evidence from Rb–Sr, Sm–Nd systematics, and SHRIMP dating. Journal of Geology 105, 645–656.

Simmat, R., Raith, M.M., 2008. Th–U–Pb monazite geochronometry of the Eastern Ghats Belt, India: timing an spatial disposition of poly-metamorphism. Precambrian Research 162, 16–39.

Subbarao, M.V., Charan, S.N., Divakar Rao, V., 1998. Geochemical signature of the charnockite suite rocks of the Machkund Region, Orissa: Implication for their petrogenesis and constraints on the evolutionary processes of the Eastern Ghats Mobile Belt. Geological Survey of India. Special Publication (Proceedings) 44, 256–267.

Unrug, R., 1996. The assembly of Gondwanaland. Episodes 19, 11–20.

Upadhyay, D., 2008. Alkaline magmatism along the southeastern margin of the Indian shield: implications for regional geodynamics and constraints on craton-Eastern Ghats Belt suturing. Precambrian Research 162, 59–69.

Vijaya Kumar, K., Leelanandam, C., 2008. Evolution of the Eastern Ghats Belt, India: a plate tectonic perspective. Journal of Geological Society of India 72, 720–749.

Walker, T.L., 1902. Geology of Kalahandi State, Central Provinces. Memoir, Geological Survey of India 33, Part 3.

Zhao, G.C., Cawood, P.A., Wilde, S.A., Sun, M., 2002. Review of global 2.1–1.8 Ga orogens: implications for a pre-Rodinia supercontinent. Earth Science Review 59, 125–162.